Elsevier Editorial System(tm) for Water Research + OA Mirror

Manuscript Draft

Manuscript Number: WR45419R2

Title: Combining electrokinetic transport and bioremediation for enhanced removal of crude oil from contaminated marine sediments: results of a long-term, mesocosm-scale experiment

Article Type: Research Paper

Keywords: Crude oil; Electrobioremediation; Electrokinetic remediation; Marine sediments

Corresponding Author: Dr. Federico Aulenta, PhD

Corresponding Author's Institution: National Research Council

First Author: Simone Cappello

Order of Authors: Simone Cappello; Carolina Cruz Viggi; Michail Yakimov; Simona Rossetti; Bruna Matturro; Lazaro Molina; Ana Segura; Silvia Marqués; Luis Yuste; Emma Sevilla; Fernando Rojo; Angela Sherry; Obioma K Mejeha; Ian M Head; Linus Mattias Valdemar Malmquist; Jan H. Christensen; Nicolas Kalogerakis; Federico Aulenta, PhD

Abstract: Marine sediments represent an important sink of harmful petroleum hydrocarbons after an accidental oil spill. Electrobioremediation techniques, which combine electrokinetic transport and biodegradation processes, represent an emerging technological platform for a sustainable remediation of contaminated sediments. Here, we describe the results of a long-term mesocosm-scale electrobioremediation experiment for the treatment of marine sediments contaminated by crude oil. A dimensionally stable anode and a stainless-steel mesh cathode were employed to drive seawater electrolysis at a fixed current density of 11 A/m2. This approach allowed establishing conditions conducive to contaminants biodegradation, as confirmed by the enrichment of Alcanivorax borkumensis cells harboring the alkB-gene and other aerobic hydrocarbonoclastic bacteria. Oil chemistry analyses indicated that aromatic hydrocarbons were primarily removed from the sediment via electroosmosis whereas low molecular weight alkanes (nC6 to nC10) via biodegradation.

Combining electrokinetic transport and bioremediation for enhanced removal of crude oil from contaminated marine sediments: results of a long-term, mesocosm-scale experiment

S. Cappello[1,*], C. Cruz Viggi[2,*], M. Yakimov[1], S. Rossetti[2], B. Matturro[2], L. Molina[3], A. Segura[3], S. Marqués[3], L. Yuste[4], E. Sevilla[4], F. Rojo[4], A. Sherry[5], O.K. Mejeha[5], I.M. Head[5], L. Malmquist[6], J. H. Christensen[6], N. Kalogerakis[7], F. Aulenta[2,**]

[1] Institute for Coastal Marine Environment (IAMC), National Research Council (CNR), Messina, Italy

[2] Water Research Institute (IRSA), National Research Council (CNR), Monterotondo (RM), Italy

[3] Environmental Protection Department, Estación Experimental del Zaidín, Consejo Superior de Investigaciones Científicas (CSIC), Granada, Spain

[4] Departamento de Biotecnología Microbiana, Centro Nacional de Biotecnología, Consejo Superior de Investigaciones Científicas (CSIC), Madrid, Spain

[5] School of Civil Engineering and Geosciences, Newcastle University, Newcastle upon Tyne, United Kingdom

[6] Department of Plant and Environmental Sciences, University of Copenhagen, Copenhagen, Denmark

[7] School of Environmental Engineering, Technical University of Crete, Chania, Greece

* These Authors contributed equally to this work

** Author for correspondence. Address: IRSA-CNR, Via Salaria km 29,300, 00015 Monterotondo (RM), Italy. E-mail: aulenta@irsa.cnr.it; Tel: +39-0690672751

Abstract

Marine sediments represent an important sink of harmful petroleum hydrocarbons after an accidental oil spill. Electrobioremediation techniques, which combine electrokinetic transport and biodegradation processes, represent an emerging technological platform for a sustainable remediation of contaminated sediments. Here, we describe the results of a long-term mesocosm-scale electrobioremediation experiment for the treatment of marine sediments contaminated by crude oil. A dimensionally stable anode and a stainless-steel mesh cathode were employed to drive seawater electrolysis at a fixed current density of 11 A/m^2. This approach allowed establishing conditions conducive to contaminants biodegradation, as confirmed by the enrichment of *Alcanivorax borkumensis* cells harboring the alkB-gene and other aerobic hydrocarbonoclastic bacteria. Oil chemistry analyses indicated that aromatic hydrocarbons were primarily removed from the sediment via electroosmosis whereas low molecular weight alkanes (nC_6 to nC_{10}) via biodegradation.

Key-words: Crude oil; Electrobioremediation; Electrokinetic remediation; Marine sediments

1. Introduction

Marine sediments represent an important sink of harmful petroleum hydrocarbons (PH) after an accidental oil spill (Gong et al., 2014). A number of different chemical, physical, and microbiological processes, contribute to the sinking of PH from the water column down to the seafloor, including weathering, adsorption onto sinking particulate matter (e.g., marine snow), and the addition of chemical dispersants (Daly et al., 2016; Passow et al., 2017; Romero et al., 2017; Stout and German, 2018). Recent studies have pointed out that the fraction of spilled hydrocarbons, which ultimately reaches the seafloor may be extremely relevant, up to 14% (on a mass basis), as in the case of the Deepwater Horizon (DWH) spill (Chanton et al., 2015; Valentine et al., 2014). Upon sedimentation, PH penetrate the upper layers of the sediment whereby they can persist for years or even decades, acting as a long-lasting contamination source to natural ecosystems. The long-term persistence of hydrocarbons, buried within marine sediments, is typically due to the lack of molecular oxygen. Indeed, although extensively documented, the anaerobic biodegradation of PH typically proceeds at remarkably lower rates compared to its aerobic counterpart (Boopathy, 2017; da Cruz et al., 2011; Mapelli et al., 2017; Salminen et al., 2004). Depending on site conditions, certain oil components, such as polycyclic aromatic hydrocarbons (PAH), also tend to strongly bind onto hydrophobic sedimentary materials, particularly when they are fine-grained and constituted by clay minerals, with this process markedly reducing their bioavailability, and in turn reduced their biodegradability (Kronenberg et al., 2017; Zhao et al., 2015). Furthermore, in some cases, PH biodegradation in marine sediments may also be hampered by the lack of macro and micronutrients and/or the lack of naturally occurring hydrocarbon-degrading microorganisms (Atlas and Bartha, 1972; Singh et al., 2014).

Over the years, different strategies have been proposed, with varying degrees of success, to overcome environmental and microbiological factors rate-limiting PH biodegradation in contaminated marine sediments. As an example, addition of fertilizers and/or oxygen-

releasing compounds (e.g., calcium peroxide-based chemicals) have been considered to address nutrient and oxygen limitation issues, respectively (Boufadel et al., 1999; Mosmeri et al., 2018; Wu et al., 2018). However, difficulties in delivering the amendments into the sediments, as well as their low yield of utilization by PH-degrading microorganisms due to the rapid consumption/scavenging by side biotic and abiotic reactions, make these remediation approaches both highly expensive and scarcely effective. Furthermore, the ever-increasing attention towards environmental sustainability is now catalyzing the interest towards novel (bio)remediation technologies which involve minimal use of chemicals (and external energy) and have, accordingly, low environmental impact. In this context, electrobioremediation technologies have recently attracted considerable attention, particularly following the discovery of an ever-increasing number of microorganisms capable to degrade environmental contaminants, including PH, using electrodes as virtually inexhaustible terminal electron acceptors in their metabolism (Aulenta et al., 2009; Cruz Viggi et al., 2015; Daghio et al., 2018, 2016, 2016; Domínguez-Garay et al., 2018; Li et al., 2015; Mao et al., 2016; Modin and Aulenta, 2017; Rakoczy et al., 2013; Rodrigo Quejigo et al., 2016; Wang et al., 2015; Zhang et al., 2010). Furthermore, bioelectrochemical system have also proved as an effective mean to manipulate the redox potential of a contaminated matrix and, thereby, establishing in situ conditions that are conducive to contaminants biodegradation (Barba et al., 2018; Yan et al., 2015; Yan and Reible, 2015, 2012). As an example, in a previous microcosm study, dimensionally stable anodes (DSA) buried within a contaminated sediment where successfully employed to fine-tune oxygen generation within the sediment, via (low voltage, i.e., 2V) seawater electrolysis, and by so doing accelerating (up to 3-times relative to non-electrified controls) the biodegradation of crude oil hydrocarbons (Bellagamba et al., 2017).

Further to their role as direct or indirect (via oxygen generation) electron acceptors, electrodes can also be exploited to enhance PH bioavailability. Indeed, application of low-voltage direct electric currents triggers electrokinetic transport phenomena such as

95 electroosmosis, electromigration, and electrophoresis (Acar et al., 1995; Acar and
96 Alshawabkeh, 1993). In the case of non-ionic contaminants, such as PH, electroosmosis is the
97 principal transport mechanism (Kuppusamy et al., 2017; Lim et al., 2016; Luo et al., 2005).
98 Electroosmosis, or electroosmotic flow, is the movement of pore water within the
99 soil/sediment from the anode to the cathode under the influence of an electrical potential.
100 Importantly, the electroosmotic flow is directly proportional to the applied electrical gradient
101 (V/cm), but it is virtually independent of the soil/sediment porosity and hydraulic
102 conductivity, thereby making this remediation approach ideally suited for the removal of non-
103 ionic contaminants from low-permeability soils and sediments. The principles of
104 electrokinetics and electrokinetic remediation have been reviewed in several previous studies
105 (Acar et al., 1995; Acar and Alshawabkeh, 1993; Lim et al., 2014).
106 Here, we examined the viability of an integrated remediation approach, exploiting the
107 synergistic effect of electrokinetic transport and bioremediation, for the treatment of marine
108 sediments contaminated by crude oil. For the first time, the study was carried out in a highly
109 representative environmental setting based on the use of large-scale mesocosm facilities and
110 involved the application of a highly comprehensive suite of chemical, microbiological and
111 electrochemical tools and analytical techniques to assess the overall viability and
112 sustainability of the proposed approach.
113

114 **2. Materials and Methods**

115 *2.1 Experimental setup and operational conditions*

116 The hereafter described mesocosm experiments were setup and conducted at the Messina site
117 of IAMC-CNR, located on the seaside of Messina harbor (Italy). The mesocosms consisted of 2
118 Perspex tanks (length: 100 cm, depth: 30 cm; height: 40 cm), one equipped with electrodes
119 (electrolytic mesocosm) and one without electrodes (control) (Figure 1). Each tank was filled
120 with approximately 130 kg of marine sediments that were artificially contaminated in the

laboratory with Danish Underground Consortium (DUC) Light Crude Oil, to a final concentration of approximately 10 g/Kg. The main organic components of the oil were paraffins (12.7 % wt/wt), napthenes (14.6 % wt/wt), and aromatics (4.8% wt/wt). The two tanks were positioned within a larger tank (500 x 150 x 50 cm) that was kept under a continuous-flow of seawater, taken directly from the Messina harbor, at a flow rate of approximately 510 L/h. Prior to be introduced within the tank the seawater was filtered through a 200 µm nylon mesh to remove large metazoans and other suspended materials.

Figure 1.

Electrodes employed in the electrolytic mesocosm were a rectangular titanium-mesh anode coated with Ru/Ir oxides (Magneto Special Anodes, The Netherlands) and a Stainless steel 304 mesh cathode (Alpha Aesar, USA). The projected area of the cathode and the anode was approximately 0.045 m^2. The anode was positioned close to the bottom of the tank, whereas the cathode was placed in the overlying water (outside the sediment) (Figure 1). The electrodes were connected to a power source (Manson NSP-2050, Manson Engineering Industrial, Hong Kong), using Ti wires. The spacing between the anode and cathode was approximately 30 cm.

Upon setup, the electrolytic systems were maintained for approximately 2 weeks at open circuit (i.e., the electrodes kept disconnected), until the establishment of anoxic conditions within the sediment. Thereafter, the electrodes were connected to the power source and, after an initial start-up period of 14 days (aimed at verifying the electrochemical functionality of the system as a whole) during which a fixed voltage difference of 2.5 Volts was applied between the electrodes, a fixed current of 500 mA was continuously applied to the circuit. Assuming a 100% Faradic efficiency for seawater electrolysis (with oxygen evolution at the

147 anode and hydrogen evolution at the cathode being the only reactions taking place at the
148 electrodes), this applied current would theoretically correspond to an oxygen generation rate
149 of approximately 4 grams per day.
150 The electrolytic and the control mesocosms were monitored for a period of approximately
151 230 days, during which a number of analytical, electrochemical, and microbiological
152 parameters were analyzed. Notably, since one of the main objectives of the experiment was to
153 assess the radius-of-influence of the electrobioremediation system, the 2 mesocosms were
154 sampled in different positions, at increasing distance from the electrodes, with each position
155 being identified with a code (E1, E3, E5 and C1, C3, C5, for the electrolytic and the control
156 mesocosm, respectively) (Figure 2).
157 At each sampling time, sediment samples (each of approximately 50 grams) were removed
158 from the mesocosms at the different sampling positions, using a stainless steel corer and were
159 analyzed for: (i.) oil hydrocarbons by gas-chromatography mass-spectrometry (GC-MS) and
160 by ad-hoc developed biosensors; a functional gene (alkB) involved in aerobic hydrocarbons
161 biodegradation by catalyzed reported deposition – fluorescence in situ hybridization (CARD-
162 FISH); the microbial community composition using Next Generation Sequencing (NGS).
163 Throughout the study, electrochemical measurements (i.e., electric current and voltage
164 difference between electrodes) were taken directly from the power source (Manson NSP-
165 2050, Manson Engineering Industrial, Hong Kong). In correspondence to each sampling time,
166 the redox potential of the sediment was measured by inserting electrodes directly within the
167 sediment, at a depth of approximately 15 cm from the surface. A further detailed description
168 of individual analytical and microbiological methods is included in the following paragraphs.
169
170
171 **Figure 2.**
172

173

174 *2.2 Analysis of aromatic and aliphatic oil hydrocarbons by GC-MS and changes in diagnostic*
175 *ratios*

176 *2.2.1 Sample preparation.*

177 All sediment samples were homogenized with equal amounts of hydromatrix® (Agilent) in an
178 IKA 11® sample mill and extracted through pressurized liquid extraction in an ASE200 system
179 (Dionex, USA). The extraction cell for the sediment samples contained 4 grams of activated
180 silica (bottom layer), 5 grams of sample mix, topped off with Ottawa sand. The samples were
181 added 200 µL of an 8 µg/mL internal standard mix (see Table S1 for content and application).
182 The following extraction parameters were used: Pressure: 1500 psi, pre-heat time: 2 minutes,
183 static time: 5 minutes, flush volume: 70%, purge time: 60 seconds, static cycles: 2,
184 temperature: 100°C, solvent mixture: n-pentane:dichloromethane (90:10). Each cell was
185 extracted twice into separate collection vials, and after concentrating under an elevated
186 temperature (40°C), the two extracts were combined and evaporated to dryness, and
187 reconstituted to 5 mL with n-pentane:dichloromethane (90:10) and 200 µL of 8 µg/mL
188 recovery standard mix (see table S1 for content and application).

189

190 *2.2.2 GC-MS analysis*

191 The extracts were analysed using an Agilent 5975C inert XL MSD with electron ionization
192 operating in selected ion monitoring (SIM) mode, as previously described (Gallotta and
193 Christensen, 2012). In brief, the GC was equipped with a HP-5 capillary column (60 m lenght,
194 0.25 mm I.D., 0.25 µm film thickness) capillary column, with helium being used as carrier gas
195 at a flow rate of 1.1 mL/s. Aliquots of 1 µL were injected in splitless mode with injection
196 temperature of 300 °C. The column temperature programme was as follows: Initial
197 temperature 40 °C held for 2 min, 25 °C/min to 100 °C then followed by an increase of
198 5 °C/min to 315 °C (held for 14 min). The transfer line, ion source and quadrupole

temperatures were 315 °C, 230 °C and 150 °C, respectively. A total of 55 mass-to-charge ratios (m/z's) divided into 12 groups were acquired in SIM mode (Table S2). The dwell time for each m/z was 25 ms. The number of monitored ions (13 m/z's) was consistent between groups to avoid differences in the scanning frequency. Peaks were quantified using Chemstation V2.0 (Agilent technologies, Inc.).

2.3 Analysis of aromatic and low MW aliphatic hydrocarbons with biosensors

The bacterial strains used as biosensors were *Alcanivorax borkumensis* SK2 (pKSB1), which responds to *n*-alkanes having between 6 and 10 carbon atoms (Sevilla et al., 2015); *A. borkumensis* SK2 (pKSP450-3.3), which responds to pristane but not to *n*-alkanes (Sevilla et al., 2017); *Pseudomonas putida* KT2440 (pKST-1), which allows detecting benzene, toluene and xylene (Hernández-Sánchez et al., 2016); and *Novosphingobium* sp. HR1a (pKSR-1), a strain that responds to the polycyclic aromatic compounds biphenyl, naphthalene, phenanthrene and 2-methylnaphthalene (Segura et al., 2017). In all cases, the strains contained a plasmid in which the gene coding for the Green Fluorescent Protein (GFP) is transcribed from a suitable promoter whose expression is induced in the presence of specific hydrocarbon compounds; induction is achieved by means of a specific regulatory protein that senses the presence of a given hydrocarbon and responds by activating the corresponding promoter. The amount of GFP produced can be easily monitored measuring the fluorescence emitted by the cells (see below). *A. borkumensis* strains were cultured in ONR7a artificial seawater medium containing 1% (w/v) pyruvate as the carbon source (Dyksterhouse et al., 1995), while *P. putida* and *Novosphingobium* were cultured in mineral salts M9 medium (Abril et al., 1989) amended with 5 mM glucose as the carbon source. Antibiotics were added to assure the stable maintenance of the reporter plasmids (50 μg/ml streptomycin for *A. borkumensis* and *P. putida* strains, and 30 μg/ml gentamycin for *Novosphingobium*).

Assays were performed adapting previously described protocols (Hernández-Sánchez et al., 2016; Sevilla et al., 2015). Briefly, for the detection of *n*-alkanes or pristane, cultures of the *A. borkumensis* reporter strains were cultivated to stationary phase in ONR7a-pyruvate at 30°C and cells were centrifuged and re-suspended in fresh medium. After adjusting the turbidity of the culture to 0.1 (A_{600} nm) with fresh medium, 4 mL of the cell suspension were loaded into 4.5 mL crew-cap glass vials containing 0.05 g of the sediment sample, or no sample (as control). The vials were closed to avoid evaporation of the hydrocarbons and incubated at 30°C with agitation for 4 to 24 h, as specified. Vials containing the sediment samples, but lacking cells were used as blanks. To measure the fluorescence (amount of GFP) of the samples, 200 µL (in triplicate) were taken from the vials and dispensed onto a black, clear–bottomed microtiter plate. The fluorescence (excitation 480 nm, emission 520 nm) and absorbance (600 nm) were recorded simultaneously in a TECAN (CH) reader for microtiter plates equipped with a fluorescence detector. The fluorescence signal was normalized by the number of cells present, which was calculated from the turbidity of the culture (A_{600}) after detracting the turbidity of the sample with no cells. The fluorescence induction ratio was obtained by dividing the normalized fluorescence of sediment-containing samples by that of control samples containing no sediment. Three biological replicates were performed.

When using the *P. putida* or *Novosphingobium* reporter strains to detect aromatic compounds, cells were grown overnight on M9-glucose medium and then diluted in 10 ml of the same fresh medium to a turbidity (A_{600} nm) of 0.1. Cells were transferred to an Erlenmeyer flask equipped with a screw cap and 0.5 g of sediment sample were added. As control, a culture of the reporter strain was used without addition of sediment sample. Flasks were tightly closed and incubated at 30°C for 7.5 h with agitation. Two ml of the cultures were taken, centrifuged (2000 rpm) to eliminate sediments, and the turbidity (A_{600} nm) of supernatants was measured and adjusted to 0.1. Fluorescence (excitation 485 nm, emission 510 nm) was then measured in a LPS-220B fluorometer (Photon Technology International). Fluorescence values are given

as fluorescence induction ratio (fluorescence emitted in presence of sediment divided by the fluorescence emitted by the control culture without sediment). Three independent replicates were performed.

2.4 Analysis of alkB gene by CARD-FISH

Sediment samples (corresponding to 2.5-15 g of wet sediment), collected from each mesocosm, were immediately fixed with formaldehyde (2%) for 3 h, at 4 °C. Cells were extracted from sediment particles in formaldehyde-fixed samples using a cell separation method based on density gradient centrifugation (Barra Caracciolo et al., 2005). Different aliquots of the supernatant containing the detached cells were filtered through 0.2 μm filters (Ø 25 mm, Millipore) using a gentle vacuum (<0.2 bar). At least two different filters were prepared for each sample. Filters were stored at -20 °C until the hybridization assays were performed. GeneCARD-FISH assay was conducted on small filter sections according to a previously described protocol (Matturro et al., 2016). Hybridized cells carrying the alkB2 gene were visualized by epifluorescence microscopy (Olympus, BX51) and quantified by counting fluorescent cells (at least 100 cells per grid) on random grids on the filter sections. Quantitative data were expressed as cell numbers per g dry weight of sediment.

2.5 Microbial Community Analysis with Next Generation Sequencing

Forty-eight 16S rRNA amplicon libraries were generated representing communities from the sediment used to prepare the electrolytic and control mesocosms prior to incubation at increasing distance from the electrode (day 0 - E1, E3, E5 and day 0 - C1, C3, C5 respectively). The microbial communities were also characterized in sediments from the electrolytic and control mesocosms following 77 days incubation at only two distances (day 77 - E1, E5 and day 77 – C1, C5) and at 135 days of incubation at all distances from the electrode (day 135 - E1, E3, E5 and day 135 – C1, C3, C5) (n=3 for all treatments). The microbial community

analysis was conducted according to detailed procedures reported elsewhere. Briefly, DNA extraction: Extractions were performed in triplicate from sediment samples (~400 mg) using a PowerSoil® DNA Isolation Kit (Mo Bio Laboratories Inc., USA) with a ribolyser (FastPrep-24, MP Biomedicals, USA). Procedural blanks were performed to ensure extracts remained contamination-free throughout the extraction procedure.

PCR amplification 16S rRNA genes and PCR product purification: The variable V4/V5 region of the 16S rRNA gene was amplified using the degenerate primers, 515F (GTG-NCA-GCM-GCC-GCG-GTA-A) and 926R (CCG-YCA-ATT-YMT-TTR-AGT-TT) (Quince et al., 2011). PCR reactions and conditions, according to a previous study, were performed in a thermal cycler (Techne TC-512, Bibby Scientific Limited). Products were analyzed by gel electrophoresis with 1% (w/v) agarose gel in 1 x Tris-acetate EDTA buffer at 100 V for 45 min. Gels were stained with ethidium bromide and visualized with a BioSpectrum Imaging System with VisionWorks LS software (UVP, Cambridge, UK). PCR products were purified with Agencourt AMPure XP PCR purification kit (Beckman Coulter).

DNA quantification and Ion Torrent DNA sequencing: Purified DNA was quantified on a Qubit 2.0 Fluorometer (Invitrogen) with a dsDNA high sensitivity assay kit (Invitrogen). The final concentration of DNA was adjusted to 100 pM, and equimolar concentrations of DNA from all samples were pooled. The pooled amplicon library was sequenced on an Ion Torrent Personal Genome Machine (Life Technologies). The library was diluted (26 pM) and emulsion PCR performed on a OneTouch2 instrument with an Ion PGM Template OT2 400 kit according to the manufacturer's instructions (Life Technologies). Beads with bound template DNA were purified on a OneTouch ES system (Life Technologies). Following enrichment, the beads were loaded onto a PGM 316 chip and sequenced in accordance with the manufacturer's instructions.

Data analysis: Raw sequence reads were retrieved using the Torrent Suite Software V4.0 (Life Technologies). Sequence reads with a modal length of 428 bp were analyzed in QIIME

(Caporaso et al., 2010b). Sequences were assigned to samples based on their unique barcodes and simultaneously filtered to remove reads with no corresponding barcode, reads without the correct primer sequence and poor-quality reads (those with a quality score of <20 were discarded). Operational taxonomic unit (OTU) classifications were performed using UClust (Edgar, 2010), with an OTU threshold defined at 97% sequence identity. OTUs were first clustered open reference against the Greengenes 16S rRNA core alignment (DeSantis et al., 2006) and then clustered de novo. Taxonomy was assigned using RDP Classifier (Wang et al., 2007) and sequences aligned using PyNAST (Caporaso et al., 2010a). Chimeric sequences were identified with ChimeraSlayer (Haas et al., 2011) and removed before subsequent analysis. The average number of reads in individual binned libraries after filtering was 44,594 with a range from 6.0 to 130,733 reads. Libraries were rarefied to 9976 reads for comparative analysis, which excluded 2 samples from the dataset (Day 0 E1 Replicate 2, 6.0 sequences and Day 135 E1 Replicate 2 due to non-amplification during PCR) (Table S3). Core diversity analysis was subsequently performed in QIIME v1.8 to provide a comparative analysis of the microbial communities between samples. Sequences have been deposited in the NCBI's Sequence Read Archive (SRA) under BioProject PRJNA435930. Operational taxonomic unit (OTU) frequencies were subsequently used to calculate Bray-Curtis similarity indices (Bray and Curtis, 1957) for pairwise comparisons of DNA sequencing profiles. Bray-Curtis similarity values of microbial communities from electrolytic and control mesocosms were compared by non-metric multidimensional scaling (nMDS) analysis using PRIMER v7.0.13 (Clarke and Gorley, 2015).

3. Results

3.1 Electrochemical measurements

Figure 3A shows the time profiles of electric current and cell voltage throughout the whole experimental period. Remarkably, during steady-state operation of the electrolytic mesocosm

328 at a fixed current (I) of 500 mA (corresponding to a current density of 11 A/m^2), the cell
329 voltage (V) remained stably below 4.5 V, hence pointing to a low electrical resistance of the
330 system as a whole (<10 Ω), which was most likely ensured by the high electric conductivity of
331 the seawater. Accordingly, under steady-state conditions, electric power consumption (W= I x
332 V) was lower than 2.25 W.
333
334 **Figure 3.**
335
336
337 The application of a fixed current of 500 mA markedly affected the redox potential (ORP) of
338 the sediment, consistently with the occurrence of electrolytic oxygen generation at the anode
339 (Figure 3B). In the electrolytic mesocosm, at the start of the experiment the ORP was around 0
340 V vs. Ag/AgCl, then it gradually increased at all sampling points during the initial 120 days of
341 operation, before stabilizing, or slightly decreasing during the remainder of the test.
342 Specifically, at E1, the sediment redox potential reached a peak of +320 mV, after 77 days of
343 operation (i.e., t1), whereas at E3 (i.e., positioned 30 cm apart from E1) and at E5 (positioned
344 60 cm apart from E1), the redox potential reached lower peak values of +310 V and +220 V,
345 respectively, only after 135 days of operation. From day 120 onward, a slow decrease in the
346 redox potential was observed at all sampling points. At the end of the study, however, the
347 redox potential remained between +250 mV (at E1 and E3) and +150 mV (at E5).
348 A strikingly different trend was observed in the control mesocosm, whereby after a period of
349 around 120 days during which the redox potential remained nearly stable at around 0 V, it
350 gradually decreased down to -200 mV by the end of the study, suggesting the establishment of
351 anoxic conditions, most likely driven by the metabolic activity of naturally-occurring sulfate
352 reducing microorganisms.

Collectively, these results provide a clear indication that application of low-voltage direct current, prompting seawater electrolysis, allows increasing the redox potential of the sediment, thereby creating conditions that are potentially conducive for the aerobic biodegradation of oil hydrocarbons. Most importantly, the effect of electrolysis was apparent even at a distance of over 45 cm from the edge of the anode, and also in the presence of a continuous flow of seawater over the surface of the sediment.

3.2 GC-MS analysis of aromatic and aliphatic hydrocarbons

As far as the concentration of main oil components is concerned, Figure 4 shows the hopane-normalized concentration of C_0-C_4-alkylated PAHs (naphthalenes, fluorenes, dibenzothiophenes, pyrenes, and chrysenes) in the electrolytic mesocosm, at the different sampling times (t1, t2, t3) and locations (E1, E3, E5), relative to the individual t0 samples, measured in %.

Figure 4.

Although, experimental data appeared to be affected by a substantial variability, most likely caused by the intrinsic heterogeneity of the sediment material and uneven distribution contaminants, a time-dependent decrease in the content of nearly all PAHs and methylated PAHs was apparent in sediment samples taken just over the anode (i.e., sampling point E1), with removal efficiencies ranging from 80% to 100% at the last sampling time. Substantial, though incomplete, removal of PAHs was also observed in E3, located approximately 15 cm apart from the edge of the anode. By contrast, negligible removal of PAHs was observed in

samples taken at E5, with concentrations measured at the last sampling time (i.e., t3), in some cases even exceeding those detected at time zero (i.e., t0) (Figure 4).

As far as the Control experiment is concerned, negligible removal of PAHs was observed over time, at all sampling locations (Figure 5), with concentrations measured at the end of the study being typically equal or higher than those detected at t0. This latter finding provides a straightforward indication that the observed removal of PAHs in the electrolytic mesocosm was driven by the application of electric current.

Figure 5.

As far as the aliphatic hydrocarbons (nC_{13} to nC_{30}) are concerned, in the electrolytic mesocosm a time-dependent decrease in their concentrations (relative to t0) was observed almost exclusively at E1, whereas negligible changes were detected at further distance from the electrode (i.e., at E3 and E5) (Figure S1). Unexpectedly, the extent of removal of individual aliphatic hydrocarbons at E1 apparently increased with the length of the carbon chain, eventually reaching 45% in the case of nC_{30} (Figure S1).

In agreement with what observed in the case of PAHs, negligible removal of aliphatic hydrocarbons, irrespective of the chain length, was observed at all sampling locations in the control mesocosm (Figure S2), hence providing an additional line of evidence that the observed removal of hydrocarbons was triggered by the applied electric current.

3.3 Analysis of aromatic and aliphatic hydrocarbons with biosensors

Sediment samples from the electrolytic and the control mesocosms were also analyzed for target aromatic and aliphatic hydrocarbons by means of *ad hoc* developed biosensors. Besides

permitting the quantification of low molecular weight compounds that could not be analyzed via GC-MS (i.e., nC_6 to nC_{10} aliphatic hydrocarbons), biosensors also allowed an integral assessment of the progress of the bioremediation process from the quantification of lumped parameters (e.g., total PAHs). Figure 6A shows the normalized response of the biosensors for aliphatic compounds to samples taken from the electrolytic and the control mesocosms at different times (t0, t1, t2, t3). The biosensor targeting nC_6-nC_{10} indicated no apparent removal of hydrocarbons in the control mesocosm, with concentrations measured at the last sampling time (t3) being very similar or even higher than those measured at t0. A different situation was observed in the electrolytic mesocosm, with a consistent disappearance of contaminants being detected over time in the E1 sample and, though less clearly, also in sample E3. By contrast, negligible removal of nC_6-nC_{10} was observed in E5. As far as the biosensor for pristane is concerned (Figure 6B), no apparent removal was noticed both in the electrolytic and in the control mesocosm, in agreement with GC-MS data (data not shown).

Figure 6.

Figure 7 reports the results of the biosensors for aromatic hydrocarbons. Also in this case, in agreement with the results of oil chemistry obtained via GC-MS analysis, the biosensor detected a substantial time-dependent removal of aromatic hydrocarbons (i.e., BTX and PAH) in the electrolytic mesocosm only, and specifically in correspondence of E1, whereas lower to no-removal was detected at E3 and E5 and in the Control experiment.

Figure 7.

3.4 Diagnostic ratios and PAHs plots

In order to gain a deeper understanding of the prevalent oil hydrocarbons removal mechanisms (i.e., removal via electroosmosis vs. biodegradation), a number of key diagnostic ratios were calculated, from GC-MS oil chemistry analyses, for each sample and were normalized to the same ratio as measured in the original oil. Conventionally, it is assumed that, due to the different intrinsic biodegradability of the different oil components, the progress of biodegradation would result in a gradual decrease of these specific ratios. As an example, pristane (Pr) and phytane (Ph) are known to degrade at a slower rate compared to nC_{17} and nC_{18}. Therefore, it is expected that, upon biodegradation the specific ratios nC_{17}/Pr and nC_{18}/Ph would diminish over time. Same considerations apply for aromatic compounds. By contrast, removal mechanisms not linked to biodegradation, such as electroosmosis-driven mass transport, would proceed at comparable rates for compounds having similar structures such as nC_{17} and Pr and therefore, would not result in a net decrease of the corresponding diagnostic ratio. A detailed description of all diagnostic ratios herein calculated can be found elsewhere (Scheibye et al., 2017). For E1 samples, due to the extensive removal of most hydrocarbons, some diagnostic ratio became undetectable at the last sampling time (t3) (Figure S3). For some others, such as nC_{17}/Pr, and 2MN/1MN a little decrease (<10%) was observed over the course of the experiment (Figure S3). In the case of E3 and E5 samples, in which the extent of hydrocarbons removal was substantially lower than in E1 due to the greater distance from the anode, all diagnostic ratios could be calculated, and none displayed a substantial time-dependent reduction. Same considerations also apply to the control experiment, whereby all diagnostic ratios remained virtually unchanged over time. Taken as a whole, these findings suggest that, under the experimental conditions applied in this study, in the electrolytic mesocosm, removal of PAH and nC_{13}-nC_{30} was mainly due to electroosmosis rather than to biodegradation.

According to the Helmholtz-Smoluchowsky equation (Alshawabkeh et al., 1999; Cameselle and Reddy, 2012), the electroosmotic flow from the anode to the overlying cathode was estimated to be around 250 mL/d (assuming a coefficient of electroosmotic conductivity of 5×10^{-9} $m^2/V\ s$). Taking into account that the herein used sediment was "freshly" contaminated and therefore PAH were only loosely bound to the sediment material, it is plausible that in the presence of such a relatively high electroosmotic flow, the electrokinetic transport proceeded at substantially higher rates compared to aerobic biodegradation. Possibly, a different scenario could be expected in the case of "historically" contaminated sediments and/or in the presence of a more active indigenous hydrocarbonoclastic microbial community.

By contrast, with specific reference to lower MW alkanes, biosensor analyses indicated a remarkable reduction in their concentration levels which was not mirrored by a corresponding reduction in the concentration level of pristane. Therefore, under the assumption that the physico-chemical behavior of nC_6 to nC_{10} is somewhat similar to that of pristane, it seems likely that biodegradation was the primary removal mechanism for such oil components, although further lines of evidence are warranted.

The finding that electroosmosis was less effective in removing aliphatics with respect to PAHs is a somewhat unexpected finding that, however, could be related to their lower affinity for water (i.e., higher octanol/water partition coefficient). Being less prone to be removed via electroosmosis, these contaminants remained within the tanks for longer period of times. Under such conditions, aerobic biodegradation apparently assumed a more relevant role, especially in the case of low molecular weight alkanes (i.e., nC_6 to nC_{10}),

3.5 Microbiological analyses (Next Generation Sequencing and CARD-FISH detection of alkB-gene carrying cells)

Sediment samples taken at different times (t0 to t2) and positions (E1 to E5 and C1 to C5) from the electrolytic and control mesocosms were also analyzed by next-generation sequencing for identifying the dynamics of the main microbial community members, as well as, their spatial distribution (Figures 8, 9 and S5).

Figure 8.

Bray-Curtis similarities were calculated from 16S rRNA gene sequencing profiles and non-metric multidimensional scaling (nMDS) was used to assess changes in the microbial communities in electrolytic and control mesocosms (Figure 8). At time 0, microbial communities in the electrolytic mesocosm were distinct from those in the control mesocosm (Figure 8, triangles). This finding is not surprising taking into account the substantial heterogeneity of the sediment samples as also confirmed by previously described oil hydrocarbon analyses. However, within the distinct clusters, there was high similarity between sediment communities at all locations (i.e. situated close to the anode (E1) or further from the anode (E5)), and also between replicate samples (≥60-80% similarity, Figure 8). Interestingly, microbial community compositions converged at t1 (i.e., day 77) in electrolytic (E5) and control (C1) (Figure 8) with a high relative abundance of known aerobic hydrocarbon degraders, *Alcanivorax* and *Marinobacter*, in both systems (Figure 9A, B). There were successional changes in the microbial communities over time, with marked differences between t1 and t2 electrolytic and control mesocosms. Furthermore, at t2 (i.e., day 135) there appeared to be a zone of influence surrounding the anode as shown by distinct differences in the microbial communities with increasing distance from the anode in the electrified system

(Figure 8, circles). The five most abundant phyla in the electrolytic mesocosms were *Gammaproteobacteria* (56.1% ±8.3), *Alphaproteobacteria* (10.5% ±1.4), *Bacteroidetes* (12.9% ±3.8), *Firmicutes* (7.6% ±4.9) and *Deltaproteobacteria* (3.3% ±1.1) (Figure S5). Generally, the same phyla were detected in the electrolytic and control mesocosms, however there were differences in the relative abundance of the different phyla, with a marked increase in *Deltaproteobacteria* at C5 after 135 days (Figure S5) which coincided with a decrease in redox and the establishment of anoxic conditions in the control mesocosm (Figure 3). Following a more detailed analysis of the microbial communities, an increasing relative abundance of anaerobic, thermophilic spore-forming microbes within class *Clostridia* were detected over time in the microbial communities surrounding the anode (e.g., *Thermovenabulum, Desulfotomaculum, Sporotomaculum,* E1, Figure 9C), compared to communities observed in the control mesocosm and sites situated further from the anode (C1, E3, E5 at t0, t1, t2 ≤0.0005 ±0.0002 % rel. abundance). Sulfate-reducing *Desulfotomaculum* spp. have previously been isolated from oil fields and are implicated in oil biodegradation (Guan et al., 2013; Lan et al., 2011; Leu et al., 1998; Liu et al., 2008; Rosnes et al., 1991).

Figure 9.

As far as the CARD-FISH detection and quantification of the alkB gene is concerned, experimental data revealed a remarkable time-dependent increase in the concentration of *Alcanivorax borkumensis* carrying the alkB-gene in the electrolytic mesocosm at E1 and, though to a lesser extent, also at E5, hence confirming the beneficial role of electrolysis in the stimulation of aerobic hydrocarbonoclastic communities (Figure 10). In the control experiment a small increase was noticed only at C5. Taken as a whole microbiological data

provided an additional line of evidence to previously mentioned biosensors data of the stimulatory effect of electrolysis on biodegradation of (low molecular weight) alkanes.

Figure 10.

Long-term durability of electrode materials

At the end of the 230-day experimental period, the electrodes were removed from the electrolytic mesocosm and visually examined in order to assess their structural integrity. Apparently, the integrity of the Ti-mesh anode was fully preserved (Figure 11), whereas the stainless-steel cathode appeared to be highly deteriorated with evident pitting corrosion. This finding has important economic implications, particularly in consideration of the fact that the cost of used anode material (approx. 1000€/m^2) is orders of magnitude higher than that of the stainless-steel cathode. Clearly, further studies, also involving detailed microscopic and electrochemical analyses, would be warranted to more precisely assess the impact of "aging" of electrodes on their (bio)electrochemical performance.

Figure 11.

4. Conclusive remarks

The main results of this mesocosm-scale electrobioremediation study can be summarized as follows:

- Electrobioremediation proved to be a sustainable technology to remove hydrocarbons, particularly PAHs, from contaminated sediments, being characterized by a low energy footprint and a negligible need of maintenance.

- Electrobioremediation increased the ORP of the sediment, via oxygen generation, even at distance of 60 cm from the edge of the anode, despite the low applied current density of around 10 A/m^2 and resulting electric power consumption of 2.25 W.
- Consistent with electrolytic oxygen generation, electrobioremediation resulted in a remarkable increase in the concentration of *Alcanivorax borkumensis* cells (i.e., a known aerobic hydrocarbonoclastic bacterium) carrying the alkB-gene and in the development of specialized microbial communities, as determined by NGS analysis.
- Both electroosmosis and biodegradation (though to this latter to a lesser extent) contributed to the removal of contaminants from the sediment, with their relative contribution being highly dependent on the nature of contaminants.
- Further work is warranted to identify optimal operational strategies of the electrobioremediation system which allow to synergistically exploit the contribution electrokinetic and biodegradation processes to the removal of petroleum hydrocarbons from contaminated sites, since these two mechanisms appear to be a complex function of a high number of variables including type and levels of contaminants, activity of naturally occurring microbial community and applied electrochemical conditions (e.g., current density).

Acknowledgements

This work was financially supported by the European Commission within the Seventh Framework Programme under Grant Agreement No. 312139 ("Kill-Spill: Integrated biotechnological solutions for combating marine oil spills").

References

Abril, M.A., Michan, C., Timmis, K.N., Ramos, J.L., 1989. Regulator and enzyme specificities of the TOL plasmid-encoded upper pathway for degradation of aromatic hydrocarbons and

580 expansion of the substrate range of the pathway. J. Bacteriol. 171, 6782–90.

581 Acar, Y.B., Alshawabkeh, A.N., 1993. Principles of electrokinetic remediation. Environ. Sci.
582 Technol. 27, 2638–2647. doi:10.1021/es00049a002

583 Acar, Y.B., Gale, R.J., Alshawabkeh, A.N., Marks, R.E., Puppala, S., Bricka, M., Parker, R., 1995.
584 Electrokinetic remediation: Basics and technology status. J. Hazard. Mater. 40, 117–137.
585 doi:10.1016/0304-3894(94)00066-P

586 Alshawabkeh, A.N., Yeung, A.T., Bricka, M.R., 1999. Practical Aspects of In-Situ Electrokinetic
587 Extraction. J. Environ. Eng. doi:10.1061/(ASCE)0733-9372(1999)125:1(27)

588 Atlas, R.M., Bartha, R., 1972. Degradation Atlas, R.M., Bartha, R., 1972. Degradation and
589 mineralization of petroleum in sea water: Limitation by nitrogen and phosphorous.
590 Biotechnol. Bioeng. 14, 309–318. doi:10.1002/bit.260140304and mineralization of
591 petroleum in sea water: Limitation. Biotechnol. Bioeng. 14, 309–318.
592 doi:10.1002/bit.260140304

593 Aulenta, F., Canosa, A., Reale, P., Rossetti, S., Panero, S., Majone, M., 2009. Microbial reductive
594 dechlorination of trichloroethene to ethene with electrodes serving as electron donors
595 without the external addition of redox mediators. Biotechnol. Bioeng. 103, 85–91.
596 doi:10.1002/bit.22234

597 Barba, S., López-Vizcaíno, R., Saez, C., Villaseñor, J., Cañizares, P., Navarro, V., Rodrigo, M.A.,
598 2018. Electro-bioremediation at the prototype scale: What it should be learned for the
599 scale-up. Chem. Eng. J. 334, 2030–2038. doi:10.1016/j.cej.2017.11.172

600 Barra Caracciolo, A., Grenni, P., Cupo, C., Rossetti, S., 2005. In situ analysis of native microbial
601 communities in complex samples with high particulate loads. FEMS Microbiol. Lett. 253,
602 55–58. doi:10.1016/j.femsle.2005.09.018

603 Bellagamba, M., Cruz Viggi, C., Ademollo, N., Rossetti, S., Aulenta, F., 2017. Electrolysis-driven
604 bioremediation of crude oil-contaminated marine sediments. N. Biotechnol. 38.
605 doi:10.1016/j.nbt.2016.03.003

606 Boopathy, R., 2017. Anaerobic Degradation of Petroleum Hydrocarbons in Sediments, in:
607 Current Developments in Biotechnology and Bioengineering. Elsevier, pp. 475–490.
608 doi:10.1016/B978-0-444-63664-5.00020-4

609 Boufadel, M.C., Reeser, P., Suidan, M.T., Wrenn, B.A., Cheng, J., Du, X., Huang, T.L., Venosa, A.D.,
610 1999. Optimal Nitrate Concentration for the Biodegradation of n-Heptadecane in a
611 Variably-Saturated Sand Column. Environ. Technol. 20, 191–199.
612 doi:10.1080/09593332008616808

613 Bray, J.R., Curtis, J.T., 1957. An Ordination of the Upland Forest Communities of Southern
614 Wisconsin. Ecol. Monogr. 27, 325–349. doi:10.2307/1942268

615 Cameselle, C., Reddy, K.R., 2012. Development and enhancement of electro-osmotic flow for
616 the removal of contaminants from soils. Electrochim. Acta 86, 10–22.
617 doi:10.1016/j.electacta.2012.06.121

618 Caporaso, J.G., Bittinger, K., Bushman, F.D., DeSantis, T.Z., Andersen, G.L., Knight, R., 2010a.
619 PyNAST: a flexible tool for aligning sequences to a template alignment. Bioinformatics 26,
620 266–267. doi:10.1093/bioinformatics/btp636

621 Caporaso, J.G., Kuczynski, J., Stombaugh, J., Bittinger, K., Bushman, F.D., Costello, E.K., Fierer, N.,
622 Peña, A.G., Goodrich, J.K., Gordon, J.I., Huttley, G.A., Kelley, S.T., Knights, D., Koenig, J.E.,
623 Ley, R.E., Lozupone, C.A., McDonald, D., Muegge, B.D., Pirrung, M., Reeder, J., Sevinsky, J.R.,
624 Turnbaugh, P.J., Walters, W.A., Widmann, J., Yatsunenko, T., Zaneveld, J., Knight, R., 2010b.
625 QIIME allows analysis of high-throughput community sequencing data. Nat. Methods 7,
626 335–336. doi:10.1038/nmeth.f.303

627 Chanton, J., Zhao, T., Rosenheim, B.E., Joye, S., Bosman, S., Brunner, C., Yeager, K.M., Diercks,
628 A.R., Hollander, D., 2015. Using Natural Abundance Radiocarbon To Trace the Flux of
629 Petrocarbon to the Seafloor Following the Deepwater Horizon Oil Spill. Environ. Sci.
630 Technol. 49, 847–854. doi:10.1021/es5046524

631 Clarke, K.R., Gorley, R.N., 2015. PRIMER v7: User Manual/Tutorial. PRIMER-E, Plymouth.

632 Cruz Viggi, C., Presta, E., Bellagamba, M., Kaciulis, S., Balijepalli, S.K., Zanaroli, G., Petrangeli
633 Papini, M., Rossetti, S., Aulenta, F., 2015. The "Oil-Spill Snorkel": an innovative
634 bioelectrochemical approach to accelerate hydrocarbons biodegradation in marine
635 sediments. Front. Microbiol. 6. doi:10.3389/fmicb.2015.00881

636 da Cruz, G.F., de Vasconcellos, S.P., Angolini, C.F., Dellagnezze, B.M., Garcia, I.N., de Oliveira,
637 V.M., dos Santos Neto, E. V, Marsaioli, A.J., 2011. Could petroleum biodegradation be a
638 joint achievement of aerobic and anaerobic microrganisms in deep sea reservoirs? AMB
639 Express 1, 47. doi:10.1186/2191-0855-1-47

640 Daghio, M., Espinoza Tofalos, A., Leoni, B., Cristiani, P., Papacchini, M., Jalilnejad, E., Bestetti, G.,
641 Franzetti, A., 2018. Bioelectrochemical BTEX removal at different voltages: assessment of
642 the degradation and characterization of the microbial communities. J. Hazard. Mater. 341,
643 120–127. doi:10.1016/j.jhazmat.2017.07.054

644 Daghio, M., Vaiopoulou, E., Patil, S.A., Suárez-Suárez, A., Head, I.M., Franzetti, A., Rabaey, K.,
645 2016. Anodes Stimulate Anaerobic Toluene Degradation via Sulfur Cycling in Marine
646 Sediments. Appl. Environ. Microbiol. 82, 297–307. doi:10.1128/AEM.02250-15

647 Daly, K.L., Passow, U., Chanton, J., Hollander, D., 2016. Assessing the impacts of oil-associated
648 marine snow formation and sedimentation during and after the Deepwater Horizon oil
649 spill. Anthropocene 13, 18–33. doi:10.1016/j.ancene.2016.01.006

650 DeSantis, T.Z., Hugenholtz, P., Larsen, N., Rojas, M., Brodie, E.L., Keller, K., Huber, T., Dalevi, D.,
651 Hu, P., Andersen, G.L., 2006. Greengenes, a Chimera-Checked 16S rRNA Gene Database
652 and Workbench Compatible with ARB. Appl. Environ. Microbiol. 72, 5069–5072.
653 doi:10.1128/AEM.03006-05

654 Domínguez-Garay, A., Quejigo, J.R., Dörfler, U., Schroll, R., Esteve-Núñez, A., 2018.
655 Bioelectroventing: an electrochemical-assisted bioremediation strategy for cleaning-up
656 atrazine-polluted soils. Microb. Biotechnol. 11, 50–62. doi:10.1111/1751-7915.12687

657 Dyksterhouse, S.E., Gray, J.P., Herwig, R.P., Lara, J.C., Staley, J.T., 1995. Cycloclasticus pugetii
658 gen. nov., sp. nov., an Aromatic hydrocarbon- degrading bacterium from marine
659 sediments 45, 116–123.

660 Edgar, R.C., 2010. Search and clustering orders of magnitude faster than BLAST.
661 Bioinformatics 26, 2460–2461. doi:10.1093/bioinformatics/btq461

662 Gallotta, F.D.C., Christensen, J.H., 2012. Source identification of petroleum hydrocarbons in soil
663 and sediments from Iguaçu River Watershed, Paraná, Brazil using the CHEMSIC method
664 (CHEMometric analysis of Selected Ion Chromatograms). J. Chromatogr. A 1235, 149–
665 158. doi:10.1016/J.CHROMA.2012.02.041

666 Gong, Y., Zhao, X., Cai, Z., O'Reilly, S.E., Hao, X., Zhao, D., 2014. A review of oil, dispersed oil and
667 sediment interactions in the aquatic environment: Influence on the fate, transport and
668 remediation of oil spills. Mar. Pollut. Bull. 79, 16–33.
669 doi:10.1016/j.marpolbul.2013.12.024

670 Guan, J., Xia, L.-P., Wang, L.-Y., Liu, J.-F., Mu, B.-Z., 2013. Diversity and distribution of sulfate-
671 reducing bacteria in four petroleum reservoirs detected by using 16S rRNA and dsrAB
672 genes. Int. Biodeterior. Biodegradation 76, 58–66. doi:10.1016/J.IBIOD.2012.06.021

673 Haas, B.J., Gevers, D., Earl, A.M., Feldgarden, M., Ward, D. V., Giannoukos, G., Ciulla, D., Tabbaa,
674 D., Highlander, S.K., Sodergren, E., Methe, B., DeSantis, T.Z., Petrosino, J.F., Knight, R.,
675 Birren, B.W., 2011. Chimeric 16S rRNA sequence formation and detection in Sanger and
676 454-pyrosequenced PCR amplicons. Genome Res. 21, 494–504.
677 doi:10.1101/gr.112730.110

678 Hernández-Sánchez, V., Molina, L., Ramos, J.L., Segura, A., 2016. New family of biosensors for
679 monitoring BTX in aquatic and edaphic environments. Microb. Biotechnol. 9, 858–867.
680 doi:10.1111/1751-7915.12394

681 Kronenberg, M., Trably, E., Bernet, N., Patureau, D., 2017. Biodegradation of polycyclic
682 aromatic hydrocarbons: Using microbial bioelectrochemical systems to overcome an
683 impasse. Environ. Pollut. 231, 509–523. doi:10.1016/j.envpol.2017.08.048

684 Kuppusamy, S., Thavamani, P., Venkateswarlu, K., Lee, Y.B., Naidu, R., Megharaj, M., 2017.
685 Remediation approaches for polycyclic aromatic hydrocarbons (PAHs) contaminated
686 soils: Technological constraints, emerging trends and future directions. Chemosphere
687 168, 944–968. doi:10.1016/j.chemosphere.2016.10.115

688 Lan, G., Li, Z., Zhang, H., Zou, C., Qiao, D., Cao, Y., 2011. Enrichment and diversity analysis of the
689 thermophilic microbes in a high temperature petroleum reservoir. African J. Microbiol.
690 Res. 5, 1850–1857. doi:10.5897/AJMR11.354

691 Leu, J.-Y., McGovern-Traa, C.P., Porter, A.J.., Harris, W.J., Hamilton, W.A., 1998. Identification
692 and Phylogenetic Analysis of Thermophilic Sulfate-Reducing Bacteria in Oil Field Samples
693 by 16S rDNA Gene Cloning and Sequencing. Anaerobe 4, 165–174.
694 doi:10.1006/anae.1998.0156

695 Li, X., Wang, X., Ren, Z.J., Zhang, Y., Li, N., Zhou, Q., 2015. Sand amendment enhances
696 bioelectrochemical remediation of petroleum hydrocarbon contaminated soil.

Chemosphere 141, 62–70. doi:10.1016/j.chemosphere.2015.06.025

Lim, M.W., Lau, E. Von, Poh, P.E., 2016. A comprehensive guide of remediation technologies for oil contaminated soil — Present works and future directions. Mar. Pollut. Bull. 109, 14–45. doi:10.1016/j.marpolbul.2016.04.023

Lim, S.K., Shin, H.S., Yoon, K.S., Kwack, S.J., Um, Y.M., Hyeon, J.H., Kwak, H.M., Kim, J.Y., Kim, T.H., Kim, Y.J., Roh, T.H., Lim, D.S., Shin, M.K., Choi, S.M., Kim, H.S., Lee, B.-M., 2014. Risk Assessment of Volatile Organic Compounds Benzene, Toluene, Ethylbenzene, and Xylene (BTEX) in Consumer Products. J. Toxicol. Environ. Heal. Part A 77, 1502–1521. doi:10.1080/15287394.2014.955905

Liu, Y., Nikolausz, M., Jin, P., 2008. Abundance and diversity of sulphate-reducing bacteria within a crude oil gathering and transferring system in China. Ann. Microbiol. 58, 611–615. doi:10.1007/BF03175565

Luo, Q., Zhang, X., Wang, H., Qian, Y., 2005. Mobilization of phenol and dichlorophenol in unsaturated soils by non-uniform electrokinetics. Chemosphere 59, 1289–1298. doi:10.1016/j.chemosphere.2004.11.043

Mao, D., Lu, L., Revil, A., Zuo, Y., Hinton, J., Ren, Z.J., 2016. Geophysical Monitoring of Hydrocarbon-Contaminated Soils Remediated with a Bioelectrochemical System. Environ. Sci. Technol. 50, 8205–8213. doi:10.1021/acs.est.6b00535

Mapelli, F., Scoma, A., Michoud, G., Aulenta, F., Boon, N., Borin, S., Kalogerakis, N., Daffonchio, D., 2017. Biotechnologies for Marine Oil Spill Cleanup: Indissoluble Ties with Microorganisms. Trends Biotechnol. 35. doi:10.1016/j.tibtech.2017.04.003

Matturro, B., Frascadore, E., Cappello, S., Genovese, M., Rossetti, S., 2016. In situ detection of alkB2 gene involved in Alcanivorax borkumensis SK2 T hydrocarbon biodegradation.

720 Mar. Pollut. Bull. 110, 378–382. doi:10.1016/j.marpolbul.2016.06.038

721 Modin, O., Aulenta, F., 2017. Three promising applications of microbial electrochemistry for
722 the water sector. Environ. Sci. Water Res. Technol. 3. doi:10.1039/c6ew00325g

723 Mosmeri, H., Tasharrofi, S., Alaie, E., Sadegh Hassani, S., 2018. Controlled-release oxygen
724 nanocomposite for bioremediation of benzene contaminated groundwater, in: New
725 Polymer Nanocomposites for Environmental Remediation. Elsevier, pp. 601–622.
726 doi:10.1016/B978-0-12-811033-1.00023-8

727 Passow, U., Sweet, J., Quigg, A., 2017. How the dispersant Corexit impacts the formation of
728 sinking marine oil snow. Mar. Pollut. Bull. 125, 139–145.
729 doi:10.1016/j.marpolbul.2017.08.015

730 Rakoczy, J., Feisthauer, S., Wasmund, K., Bombach, P., Neu, T.R., Vogt, C., Richnow, H.H., 2013.
731 Benzene and sulfide removal from groundwater treated in a microbial fuel cell.
732 Biotechnol. Bioeng. 110, 3104–3113. doi:10.1002/bit.24979

733 Rodrigo Quejigo, J., Dörfler, U., Schroll, R., Esteve-Núñez, A., 2016. Stimulating soil
734 microorganisms for mineralizing the herbicide isoproturon by means of microbial
735 electroremediating cells. Microb. Biotechnol. 9, 369–380. doi:10.1111/1751-7915.12351

736 Romero, I.C., Toro-Farmer, G., Diercks, A.-R., Schwing, P., Muller-Karger, F., Murawski, S.,
737 Hollander, D.J., 2017. Large-scale deposition of weathered oil in the Gulf of Mexico
738 following a deep-water oil spill. Environ. Pollut. 228, 179–189.
739 doi:10.1016/j.envpol.2017.05.019

740 Rosnes, J.T., Torsvik, T., Lien, T., 1991. Spore-forming thermophilic sulfate-reducing bacteria
741 isolated from north sea oil field waters. Appl. Environ. Microbiol. 57, 2302–7.

742 Salminen, J.M., Tuomi, P.M., Suortti, A.-M., Jørgensen, K.S., 2004. Potential for Aerobic and

743 Anaerobic Biodegradation of Petroleum Hydrocarbons in Boreal Subsurface.
744 Biodegradation 15, 29–39. doi:10.1023/B:BIOD.0000009954.21526.e8

745 Scheibye, K., Christensen, J.H., Johnsen, A.R., 2017. Biodegradation of crude oil in Arctic
746 subsurface water from the Disko Bay (Greenland) is limited. Environ. Pollut. 223, 73–80.
747 doi:10.1016/J.ENVPOL.2016.12.032

748 Segura, A., Hernández-Sánchez, V., Marqués, S., Molina, L., 2017. Insights in the regulation of
749 the degradation of PAHs in Novosphingobium sp. HR1a and utilization of this regulatory
750 system as a tool for the detection of PAHs. Sci. Total Environ. 590–591, 381–393.
751 doi:10.1016/j.scitotenv.2017.02.180

752 Sevilla, E., Yuste, L., Moreno, R., Rojo, F., 2017. Differential expression of the three *Alcanivorax*
753 *borkumensis* SK2 genes coding for the P450 cytochromes involved in the assimilation of
754 hydrocarbons. Environ. Microbiol. Rep. 9, 797–808. doi:10.1111/1758-2229.12598

755 Sevilla, E., Yuste, L., Rojo, F., 2015. Marine hydrocarbonoclastic bacteria as whole-cell
756 biosensors for *n* -alkanes. Microb. Biotechnol. 8, 693–706. doi:10.1111/1751-
757 7915.12286

758 Singh, A.K., Sherry, A., Gray, N.D., Jones, D.M., Bowler, B.F.J., Head, I.M., 2014. Kinetic
759 parameters for nutrient enhanced crude oil biodegradation in intertidal marine
760 sediments. Front. Microbiol. 5. doi:10.3389/fmicb.2014.00160

761 Stout, S.A., German, C.R., 2018. Characterization and flux of marine oil snow settling toward
762 the seafloor in the northern Gulf of Mexico during the Deepwater Horizon incident:
763 Evidence for input from surface oil and impact on shallow shelf sediments. Mar. Pollut.
764 Bull. 129, 695–713. doi:10.1016/j.marpolbul.2017.10.059

765 Valentine, D.L., Fisher, G.B., Bagby, S.C., Nelson, R.K., Reddy, C.M., Sylva, S.P., Woo, M.A., 2014.

766 Fallout plume of submerged oil from *Deepwater Horizon*. Proc. Natl. Acad. Sci. 111,
767 15906–15911. doi:10.1073/pnas.1414873111

768 Wang, H., Luo, H., Fallgren, P.H., Jin, S., Ren, Z.J., 2015. Bioelectrochemical system platform for
769 sustainable environmental remediation and energy generation. Biotechnol. Adv. 33, 317–
770 334. doi:10.1016/j.biotechadv.2015.04.003

771 Wang, Q., Garrity, G.M., Tiedje, J.M., Cole, J.R., 2007. Naive Bayesian Classifier for Rapid
772 Assignment of rRNA Sequences into the New Bacterial Taxonomy. Appl. Environ.
773 Microbiol. 73, 5261–5267. doi:10.1128/AEM.00062-07

774 Wu, H., Sun, L., Wang, H., Wang, X., 2018. *In situ* sodium persulfate/calcium peroxide oxidation
775 in remediation of TPH-contaminated soil in 3D-sand box. Environ. Technol. 39, 91–101.
776 doi:10.1080/09593330.2017.1296029

777 Yan, F., Chen, W., Reible, D., 2015. Electrochemical Stimulation of PAH Biodegradation in
778 Sediment. Soil Sediment Contam. An Int. J. 24, 143–156.
779 doi:10.1080/15320383.2014.922932

780 Yan, F., Reible, D., 2015. Electro-bioremediation of contaminated sediment by electrode
781 enhanced capping. J. Environ. Manage. 155, 154–161.
782 doi:10.1016/j.jenvman.2015.03.023

783 Yan, F., Reible, D.D., 2012. PAH degradation and redox control in an electrode enhanced
784 sediment cap. J. Chem. Technol. Biotechnol. 87, 1222–1228. doi:10.1002/jctb.3767

785 Zhang, T., Gannon, S.M., Nevin, K.P., Franks, A.E., Lovley, D.R., 2010. Stimulating the anaerobic
786 degradation of aromatic hydrocarbons in contaminated sediments by providing an
787 electrode as the electron acceptor. Environ. Microbiol. 12, 1011–1020.
788 doi:10.1111/j.1462-2920.2009.02145.x

789 Zhao, X., Gong, Y., O'Reilly, S.E., Zhao, D., 2015. Effects of oil dispersant on solubilization,
790 sorption and desorption of polycyclic aromatic hydrocarbons in sediment–seawater
791 systems. Mar. Pollut. Bull. 92, 160–169. doi:10.1016/j.marpolbul.2014.12.042

792

793

Figure legends

Figure 1. (A) Schematic representation of the mesocosm-scale electrobioremediation experiment. (B) Picture of the two mesocosms positioned one next to the other within the larger tank, kept under a continuous-flow of seawater. Picture taken during the initial filling of the larger tank.

Figure 2. Schematic representation of the two mesocosms with indication of the sampling positions. The direction of seawater flow is from E1/C1 to E5/C5, as depicted in Figure 1B.

Figure 3. (A) Current and cell voltage throughout the whole experimental period for the electrolytic mesocosm. t0= day 0; t1 =day 77; t2 = day 135; t3 = day 230. (B) Time course of the sediment redox potential in the electrolytic and in the control mesocosms.

Figure 4. Hopane-normalized concentration of C_0-C_4-alkylated PAHs in the electrolytic mesocosm, at the different sampling times (t1, t2, t3), and points (E1, E3, E5) relative to t0 samples, measured in %. Note that columns marked with asterisks are above 150% of t0.

Figure 5. Hopane-normalized concentration of C_0-C_4-alkylated PAHs in the Control experiment, at the different sampling times (t1, t2, t3), and points (C1, C3, C5) relative to the average of all t0 samples, measured in %. Note that columns marked with asterisks are above 150% of t0.

Figure 6. Response of the biosensors for (A) nC_6 to nC_{10} and (B) pristane. A fluorescence induction higher than 2-fold (red dashed line in the graphs) was considered as indicative of the presence of hydrocarbons.

Figure 7. Response of the biosensors for (A) BTX and (B) PAHs. A fluorescence induction higher than 2-fold (red dashed line in the graphs) was considered as indicative of the presence of hydrocarbons.

Figure 8. Non-metric multidimensional scaling (nMDS) of Bray-Curtis similarities of 16S rRNA gene sequencing profiles from electrolytic (E) and control (C) mesocosms. Microbial community profiles were generated at t0, 77 days (t1) and 135 days (t2) at different distances from the anode (e.g. E1, E3, E5).

Figure 9. Putative hydrocarbon-degrading microbial communities in electrolytic and control mesocosms. Relative abundance (%) of aerobic hydrocarbon degraders across all treatments (A, B) and anaerobic, thermophilic spore-formers in E1 only (C).

Figure 10. Concentration of cells carrying the alkB-gene in samples from the electrolytic and the control mesocosm.

Figure 11. Appearance of the Ti-MMO anode and the Stainless-steel cathode at the start (A, C) and at the end (B, D) of the study.

Combining electrokinetic transport and bioremediation for enhanced removal of crude oil from contaminated marine sediments: results of a long-term, mesocosm-scale experiment

S. Cappello[1,*], C. Cruz Viggi[2,*], M. Yakimov[1], S. Rossetti[2], B. Matturro[2], L. Molina[3], A. Segura[3], S. Marqués[3], L. Yuste[4], E. Sevilla[4], F. Rojo[4], A. Sherry[5], O.K. Mejeha[5], I.M. Head[5], L. Malmquist[6], J. H. Christensen[6], N. Kalogerakis[7], F. Aulenta[2,**]

[1] Institute for Coastal Marine Environment (IAMC), National Research Council (CNR), Messina, Italy

[2] Water Research Institute (IRSA), National Research Council (CNR), Monterotondo (RM), Italy

[3] Environmental Protection Department, Estación Experimental del Zaidín, Consejo Superior de Investigaciones Científicas (CSIC), Granada, Spain

[4] Departamento de Biotecnología Microbiana, Centro Nacional de Biotecnología, Consejo Superior de Investigaciones Científicas (CSIC), Madrid, Spain

[5] School of Civil Engineering and Geosciences, Newcastle University, Newcastle upon Tyne, United Kingdom

[6] Department of Plant and Environmental Sciences, University of Copenhagen, Copenhagen, Denmark

[7] School of Environmental Engineering, Technical University of Crete, Chania, Greece

* These Authors contributed equally to this work

** Author for correspondence. Address: IRSA-CNR, Via Salaria km 29,300, 00015 Monterotondo (RM), Italy. E-mail: aulenta@irsa.cnr.it; Tel: +39-0690672751

Abstract

Marine sediments represent an important sink of harmful petroleum hydrocarbons after an accidental oil spill. Electrobioremediation techniques, which combine electrokinetic transport and biodegradation processes, represent an emerging technological platform for a sustainable remediation of contaminated sediments. Here, we describe the results of a long-term mesocosm-scale electrobioremediation experiment for the treatment of marine sediments contaminated by crude oil. A dimensionally stable anode and a stainless-steel mesh cathode were employed to drive seawater electrolysis at a fixed current density of 11 A/m^2. This approach allowed establishing conditions conducive to contaminants biodegradation, as confirmed by the enrichment of *Alcanivorax borkumensis* cells harboring the alkB-gene and other aerobic hydrocarbonoclastic bacteria. Oil chemistry analyses indicated that aromatic hydrocarbons were primarily removed from the sediment via electroosmosis whereas low molecular weight alkanes (nC_6 to nC_{10}) via biodegradation.

Key-words: Crude oil; Electrobioremediation; Electrokinetic remediation; Marine sediments

1. Introduction

Marine sediments represent an important sink of harmful petroleum hydrocarbons (PH) after an accidental oil spill (Gong et al., 2014). A number of different chemical, physical, and microbiological processes, contribute to the sinking of PH from the water column down to the seafloor, including weathering, adsorption onto sinking particulate matter (e.g., marine snow), and the addition of chemical dispersants (Daly et al., 2016; Passow et al., 2017; Romero et al., 2017; Stout and German, 2018). Recent studies have pointed out that the fraction of spilled hydrocarbons, which ultimately reaches the seafloor may be extremely relevant, up to 14% (on a mass basis), as in the case of the Deepwater Horizon (DWH) spill (Chanton et al., 2015; Valentine et al., 2014). Upon sedimentation, PH penetrate the upper layers of the sediment whereby they can persist for years or even decades, acting as a long-lasting contamination source to natural ecosystems. The long-term persistence of hydrocarbons, buried within marine sediments, is typically due to the lack of molecular oxygen. Indeed, although extensively documented, the anaerobic biodegradation of PH typically proceeds at remarkably lower rates compared to its aerobic counterpart (Boopathy, 2017; da Cruz et al., 2011; Mapelli et al., 2017; Salminen et al., 2004). Depending on site conditions, certain oil components, such as polycyclic aromatic hydrocarbons (PAH), also tend to strongly bind onto hydrophobic sedimentary materials, particularly when they are fine-grained and constituted by clay minerals, with this process markedly reducing their bioavailability, and in turn reduced their biodegradability (Kronenberg et al., 2017; Zhao et al., 2015). Furthermore, in some cases, PH biodegradation in marine sediments may also be hampered by the lack of macro and micronutrients and/or the lack of naturally occurring hydrocarbon-degrading microorganisms (Atlas and Bartha, 1972; Singh et al., 2014).

Over the years, different strategies have been proposed, with varying degrees of success, to overcome environmental and microbiological factors rate-limiting PH biodegradation in contaminated marine sediments. As an example, addition of fertilizers and/or oxygen-

releasing compounds (e.g., calcium peroxide-based chemicals) have been considered to address nutrient and oxygen limitation issues, respectively (Boufadel et al., 1999; Mosmeri et al., 2018; Wu et al., 2018). However, difficulties in delivering the amendments into the sediments, as well as their low yield of utilization by PH-degrading microorganisms due to the rapid consumption/scavenging by side biotic and abiotic reactions, make these remediation approaches both highly expensive and scarcely effective. Furthermore, the ever-increasing attention towards environmental sustainability is now catalyzing the interest towards novel (bio)remediation technologies which involve minimal use of chemicals (and external energy) and have, accordingly, low environmental impact. In this context, electrobioremediation technologies have recently attracted considerable attention, particularly following the discovery of an ever-increasing number of microorganisms capable to degrade environmental contaminants, including PH, using electrodes as virtually inexhaustible terminal electron acceptors in their metabolism (Aulenta et al., 2009; Cruz Viggi et al., 2015; Daghio et al., 2018, 2016, 2016; Domínguez-Garay et al., 2018; Li et al., 2015; Mao et al., 2016; Modin and Aulenta, 2017; Rakoczy et al., 2013; Rodrigo Quejigo et al., 2016; Wang et al., 2015; Zhang et al., 2010). Furthermore, bioelectrochemical system have also proved as an effective mean to manipulate the redox potential of a contaminated matrix and, thereby, establishing in situ conditions that are conducive to contaminants biodegradation (Barba et al., 2018; Yan et al., 2015; Yan and Reible, 2015, 2012). As an example, in a previous microcosm study, dimensionally stable anodes (DSA) buried within a contaminated sediment where successfully employed to fine-tune oxygen generation within the sediment, via (low voltage, i.e., 2V) seawater electrolysis, and by so doing accelerating (up to 3-times relative to non-electrified controls) the biodegradation of crude oil hydrocarbons (Bellagamba et al., 2017).

Further to their role as direct or indirect (via oxygen generation) electron acceptors, electrodes can also be exploited to enhance PH bioavailability. Indeed, application of low-voltage direct electric currents triggers electrokinetic transport phenomena such as

electroosmosis, electromigration, and electrophoresis (Acar et al., 1995; Acar and Alshawabkeh, 1993). In the case of non-ionic contaminants, such as PH, electroosmosis is the principal transport mechanism (Kuppusamy et al., 2017; Lim et al., 2016; Luo et al., 2005). Electroosmosis, or electroosmotic flow, is the movement of pore water within the soil/sediment from the anode to the cathode under the influence of an electrical potential. Importantly, the electroosmotic flow is directly proportional to the applied electrical gradient (V/cm), but it is virtually independent of the soil/sediment porosity and hydraulic conductivity, thereby making this remediation approach ideally suited for the removal of non-ionic contaminants from low-permeability soils and sediments. The principles of electrokinetics and electrokinetic remediation have been reviewed in several previous studies (Acar et al., 1995; Acar and Alshawabkeh, 1993; Lim et al., 2014).

Here, we examined the viability of an integrated remediation approach, exploiting the synergistic effect of electrokinetic transport and bioremediation, for the treatment of marine sediments contaminated by crude oil. For the first time, the study was carried out in a highly representative environmental setting based on the use of large-scale mesocosm facilities and involved the application of a highly comprehensive suite of chemical, microbiological and electrochemical tools and analytical techniques to assess the overall viability and sustainability of the proposed approach.

2. Materials and Methods

2.1 Experimental setup and operational conditions

The hereafter described mesocosm experiments were setup and conducted at the Messina site of IAMC-CNR, located on the seaside of Messina harbor (Italy). The mesocosms consisted of 2 Perspex tanks (length: 100 cm, depth: 30 cm; height: 40 cm), one equipped with electrodes (electrolytic mesocosm) and one without electrodes (control) (Figure 1). Each tank was filled with approximately 130 kg of marine sediments that were artificially contaminated in the

laboratory with Danish Underground Consortium (DUC) Light Crude Oil, to a final concentration of approximately 10 g/Kg. The main organic components of the oil were paraffins (12.7 % wt/wt), napthenes (14.6 % wt/wt), and aromatics (4.8% wt/wt). The two tanks were positioned within a larger tank (500 x 150 x 50 cm) that was kept under a continuous-flow of seawater, taken directly from the Messina harbor, at a flow rate of approximately 510 L/h. Prior to be introduced within the tank the seawater was filtered through a 200 μm nylon mesh to remove large metazoans and other suspended materials.

Figure 1.

Electrodes employed in the electrolytic mesocosm were a rectangular titanium-mesh anode coated with Ru/Ir oxides (Magneto Special Anodes, The Netherlands) and a Stainless steel 304 mesh cathode (Alpha Aesar, USA). The projected area of the cathode and the anode was approximately 0.045 m^2. The anode was positioned close to the bottom of the tank, whereas the cathode was placed in the overlying water (outside the sediment) (Figure 1). The electrodes were connected to a power source (Manson NSP-2050, Manson Engineering Industrial, Hong Kong), using Ti wires. The spacing between the anode and cathode was approximately 30 cm.

Upon setup, the electrolytic systems were maintained for approximately 2 weeks at open circuit (i.e., the electrodes kept disconnected), until the establishment of anoxic conditions within the sediment. Thereafter, the electrodes were connected to the power source and, after an initial start-up period of 14 days (aimed at verifying the electrochemical functionality of the system as a whole) during which a fixed voltage difference of 2.5 Volts was applied between the electrodes, a fixed current of 500 mA was continuously applied to the circuit. Assuming a 100% Faradic efficiency for seawater electrolysis (with oxygen evolution at the

147 anode and hydrogen evolution at the cathode being the only reactions taking place at the
148 electrodes), this applied current would theoretically correspond to an oxygen generation rate
149 of approximately 4 grams per day.
150 The electrolytic and the control mesocosms were monitored for a period of approximately
151 230 days, during which a number of analytical, electrochemical, and microbiological
152 parameters were analyzed. Notably, since one of the main objectives of the experiment was to
153 assess the radius-of-influence of the electrobioremediation system, the 2 mesocosms were
154 sampled in different positions, at increasing distance from the electrodes, with each position
155 being identified with a code (E1, E3, E5 and C1, C3, C5, for the electrolytic and the control
156 mesocosm, respectively) (Figure 2).
157 At each sampling time, sediment samples (each of approximately 50 grams) were removed
158 from the mesocosms at the different sampling positions, using a stainless steel corer and were
159 analyzed for: (i.) oil hydrocarbons by gas-chromatography mass-spectrometry (GC-MS) and
160 by ad-hoc developed biosensors; a functional gene (alkB) involved in aerobic hydrocarbons
161 biodegradation by catalyzed reported deposition – fluorescence in situ hybridization (CARD-
162 FISH); the microbial community composition using Next Generation Sequencing (NGS).
163 Throughout the study, electrochemical measurements (i.e., electric current and voltage
164 difference between electrodes) were taken directly from the power source (Manson NSP-
165 2050, Manson Engineering Industrial, Hong Kong). In correspondence to each sampling time,
166 the redox potential of the sediment was measured by inserting electrodes directly within the
167 sediment, at a depth of approximately 15 cm from the surface. A further detailed description
168 of individual analytical and microbiological methods is included in the following paragraphs.
169
170
171 **Figure 2.**
172

2.2 Analysis of aromatic and aliphatic oil hydrocarbons by GC-MS and changes in diagnostic ratios

2.2.1 Sample preparation.

All sediment samples were homogenized with equal amounts of hydromatrix® (Agilent) in an IKA 11® sample mill and extracted through pressurized liquid extraction in an ASE200 system (Dionex, USA). The extraction cell for the sediment samples contained 4 grams of activated silica (bottom layer), 5 grams of sample mix, topped off with Ottawa sand. The samples were added 200 µL of an 8 µg/mL internal standard mix (see Table S1 for content and application). The following extraction parameters were used: Pressure: 1500 psi, pre-heat time: 2 minutes, static time: 5 minutes, flush volume: 70%, purge time: 60 seconds, static cycles: 2, temperature: 100°C, solvent mixture: n-pentane:dichloromethane (90:10). Each cell was extracted twice into separate collection vials, and after concentrating under an elevated temperature (40°C), the two extracts were combined and evaporated to dryness, and reconstituted to 5 mL with n-pentane:dichloromethane (90:10) and 200 µL of 8 µg/mL recovery standard mix (see table S1 for content and application).

2.2.2 GC-MS analysis

The extracts were analysed using an Agilent 5975C inert XL MSD with electron ionization operating in selected ion monitoring (SIM) mode, as previously described (Gallotta and Christensen, 2012). In brief, the GC was equipped with a HP-5 capillary column (60 m lenght, 0.25 mm I.D., 0.25 µm film thickness) capillary column, with helium being used as carrier gas at a flow rate of 1.1 mL/s. Aliquots of 1 µL were injected in splitless mode with injection temperature of 300 °C. The column temperature programme was as follows: Initial temperature 40 °C held for 2 min, 25 °C/min to 100 °C then followed by an increase of 5 °C/min to 315 °C (held for 14 min). The transfer line, ion source and quadrupole

temperatures were 315 °C, 230 °C and 150 °C, respectively. A total of 55 mass-to-charge ratios (m/z's) divided into 12 groups were acquired in SIM mode (Table S2). The dwell time for each m/z was 25 ms. The number of monitored ions (13 m/z's) was consistent between groups to avoid differences in the scanning frequency. Peaks were quantified using Chemstation V2.0 (Agilent technologies, Inc.).

2.3 Analysis of aromatic and low MW aliphatic hydrocarbons with biosensors

The bacterial strains used as biosensors were *Alcanivorax borkumensis* SK2 (pKSB1), which responds to *n*-alkanes having between 6 and 10 carbon atoms (Sevilla et al., 2015); *A. borkumensis* SK2 (pKSP450-3.3), which responds to pristane but not to *n*-alkanes (Sevilla et al., 2017); *Pseudomonas putida* KT2440 (pKST-1), which allows detecting benzene, toluene and xylene (Hernández-Sánchez et al., 2016); and *Novosphingobium* sp. HR1a (pKSR-1), a strain that responds to the polycyclic aromatic compounds biphenyl, naphthalene, phenanthrene and 2-methylnaphthalene (Segura et al., 2017). In all cases, the strains contained a plasmid in which the gene coding for the Green Fluorescent Protein (GFP) is transcribed from a suitable promoter whose expression is induced in the presence of specific hydrocarbon compounds; induction is achieved by means of a specific regulatory protein that senses the presence of a given hydrocarbon and responds by activating the corresponding promoter. The amount of GFP produced can be easily monitored measuring the fluorescence emitted by the cells (see below). *A. borkumensis* strains were cultured in ONR7a artificial seawater medium containing 1% (w/v) pyruvate as the carbon source (Dyksterhouse et al., 1995), while *P. putida* and *Novosphingobium* were cultured in mineral salts M9 medium (Abril et al., 1989) amended with 5 mM glucose as the carbon source. Antibiotics were added to assure the stable maintenance of the reporter plasmids (50 μg/ml streptomycin for *A. borkumensis* and *P. putida* strains, and 30 μg/ml gentamycin for *Novosphingobium*).

Assays were performed adapting previously described protocols (Hernández-Sánchez et al., 2016; Sevilla et al., 2015). Briefly, for the detection of *n*-alkanes or pristane, cultures of the *A. borkumensis* reporter strains were cultivated to stationary phase in ONR7a-pyruvate at 30°C and cells were centrifuged and re-suspended in fresh medium. After adjusting the turbidity of the culture to 0.1 (A_{600} nm) with fresh medium, 4 mL of the cell suspension were loaded into 4.5 mL crew-cap glass vials containing 0.05 g of the sediment sample, or no sample (as control). The vials were closed to avoid evaporation of the hydrocarbons and incubated at 30°C with agitation for 4 to 24 h, as specified. Vials containing the sediment samples, but lacking cells were used as blanks. To measure the fluorescence (amount of GFP) of the samples, 200 µL (in triplicate) were taken from the vials and dispensed onto a black, clear–bottomed microtiter plate. The fluorescence (excitation 480 nm, emission 520 nm) and absorbance (600 nm) were recorded simultaneously in a TECAN (CH) reader for microtiter plates equipped with a fluorescence detector. The fluorescence signal was normalized by the number of cells present, which was calculated from the turbidity of the culture (A_{600}) after detracting the turbidity of the sample with no cells. The fluorescence induction ratio was obtained by dividing the normalized fluorescence of sediment-containing samples by that of control samples containing no sediment. Three biological replicates were performed.

When using the *P. putida* or *Novosphingobium* reporter strains to detect aromatic compounds, cells were grown overnight on M9-glucose medium and then diluted in 10 ml of the same fresh medium to a turbidity (A_{600} nm) of 0.1. Cells were transferred to an Erlenmeyer flask equipped with a screw cap and 0.5 g of sediment sample were added. As control, a culture of the reporter strain was used without addition of sediment sample. Flasks were tightly closed and incubated at 30°C for 7.5 h with agitation. Two ml of the cultures were taken, centrifuged (2000 rpm) to eliminate sediments, and the turbidity (A_{600} nm) of supernatants was measured and adjusted to 0.1. Fluorescence (excitation 485 nm, emission 510 nm) was then measured in a LPS-220B fluorometer (Photon Technology International). Fluorescence values are given

as fluorescence induction ratio (fluorescence emitted in presence of sediment divided by the fluorescence emitted by the control culture without sediment). Three independent replicates were performed.

2.4 Analysis of alkB gene by CARD-FISH

Sediment samples (corresponding to 2.5-15 g of wet sediment), collected from each mesocosm, were immediately fixed with formaldehyde (2%) for 3 h, at 4 °C. Cells were extracted from sediment particles in formaldehyde-fixed samples using a cell separation method based on density gradient centrifugation (Barra Caracciolo et al., 2005). Different aliquots of the supernatant containing the detached cells were filtered through 0.2 μm filters (Ø 25 mm, Millipore) using a gentle vacuum (<0.2 bar). At least two different filters were prepared for each sample. Filters were stored at -20 °C until the hybridization assays were performed. GeneCARD-FISH assay was conducted on small filter sections according to a previously described protocol (Matturro et al., 2016). Hybridized cells carrying the alkB2 gene were visualized by epifluorescence microscopy (Olympus, BX51) and quantified by counting fluorescent cells (at least 100 cells per grid) on random grids on the filter sections. Quantitative data were expressed as cell numbers per g dry weight of sediment.

2.5 Microbial Community Analysis with Next Generation Sequencing

Forty-eight 16S rRNA amplicon libraries were generated representing communities from the sediment used to prepare the electrolytic and control mesocosms prior to incubation at increasing distance from the electrode (day 0 - E1, E3, E5 and day 0 - C1, C3, C5 respectively). The microbial communities were also characterized in sediments from the electrolytic and control mesocosms following 77 days incubation at only two distances (day 77 - E1, E5 and day 77 – C1, C5) and at 135 days of incubation at all distances from the electrode (day 135 - E1, E3, E5 and day 135 – C1, C3, C5) (n=3 for all treatments). The microbial community

analysis was conducted according to detailed procedures reported elsewhere. Briefly, DNA extraction: Extractions were performed in triplicate from sediment samples (~400 mg) using a PowerSoil® DNA Isolation Kit (Mo Bio Laboratories Inc., USA) with a ribolyser (FastPrep-24, MP Biomedicals, USA). Procedural blanks were performed to ensure extracts remained contamination-free throughout the extraction procedure.

PCR amplification 16S rRNA genes and PCR product purification: The variable V4/V5 region of the 16S rRNA gene was amplified using the degenerate primers, 515F (GTG-NCA-GCM-GCC-GCG-GTA-A) and 926R (CCG-YCA-ATT-YMT-TTR-AGT-TT) (Quince et al., 2011). PCR reactions and conditions, according to a previous study, were performed in a thermal cycler (Techne TC-512, Bibby Scientific Limited). Products were analyzed by gel electrophoresis with 1% (w/v) agarose gel in 1 x Tris-acetate EDTA buffer at 100 V for 45 min. Gels were stained with ethidium bromide and visualized with a BioSpectrum Imaging System with VisionWorks LS software (UVP, Cambridge, UK). PCR products were purified with Agencourt AMPure XP PCR purification kit (Beckman Coulter).

DNA quantification and Ion Torrent DNA sequencing: Purified DNA was quantified on a Qubit 2.0 Fluorometer (Invitrogen) with a dsDNA high sensitivity assay kit (Invitrogen). The final concentration of DNA was adjusted to 100 pM, and equimolar concentrations of DNA from all samples were pooled. The pooled amplicon library was sequenced on an Ion Torrent Personal Genome Machine (Life Technologies). The library was diluted (26 pM) and emulsion PCR performed on a OneTouch2 instrument with an Ion PGM Template OT2 400 kit according to the manufacturer's instructions (Life Technologies). Beads with bound template DNA were purified on a OneTouch ES system (Life Technologies). Following enrichment, the beads were loaded onto a PGM 316 chip and sequenced in accordance with the manufacturer's instructions.

Data analysis: Raw sequence reads were retrieved using the Torrent Suite Software V4.0 (Life Technologies). Sequence reads with a modal length of 428 bp were analyzed in QIIME

(Caporaso et al., 2010b). Sequences were assigned to samples based on their unique barcodes and simultaneously filtered to remove reads with no corresponding barcode, reads without the correct primer sequence and poor-quality reads (those with a quality score of <20 were discarded). Operational taxonomic unit (OTU) classifications were performed using UClust (Edgar, 2010), with an OTU threshold defined at 97% sequence identity. OTUs were first clustered open reference against the Greengenes 16S rRNA core alignment (DeSantis et al., 2006) and then clustered de novo. Taxonomy was assigned using RDP Classifier (Wang et al., 2007) and sequences aligned using PyNAST (Caporaso et al., 2010a). Chimeric sequences were identified with ChimeraSlayer (Haas et al., 2011) and removed before subsequent analysis. The average number of reads in individual binned libraries after filtering was 44,594 with a range from 6.0 to 130,733 reads. Libraries were rarefied to 9976 reads for comparative analysis, which excluded 2 samples from the dataset (Day 0 E1 Replicate 2, 6.0 sequences and Day 135 E1 Replicate 2 due to non-amplification during PCR) (Table S3). Core diversity analysis was subsequently performed in QIIME v1.8 to provide a comparative analysis of the microbial communities between samples. Sequences have been deposited in the NCBI's Sequence Read Archive (SRA) under BioProject PRJNA435930. Operational taxonomic unit (OTU) frequencies were subsequently used to calculate Bray-Curtis similarity indices (Bray and Curtis, 1957) for pairwise comparisons of DNA sequencing profiles. Bray-Curtis similarity values of microbial communities from electrolytic and control mesocosms were compared by non-metric multidimensional scaling (nMDS) analysis using PRIMER v7.0.13 (Clarke and Gorley, 2015).

3. Results

3.1 Electrochemical measurements

Figure 3A shows the time profiles of electric current and cell voltage throughout the whole experimental period. Remarkably, during steady-state operation of the electrolytic mesocosm

at a fixed current (I) of 500 mA (corresponding to a current density of 11 A/m^2), the cell voltage (V) remained stably below 4.5 V, hence pointing to a low electrical resistance of the system as a whole (<10 Ω), which was most likely ensured by the high electric conductivity of the seawater. Accordingly, under steady-state conditions, electric power consumption (W= I x V) was lower than 2.25 W.

Figure 3.

The application of a fixed current of 500 mA markedly affected the redox potential (ORP) of the sediment, consistently with the occurrence of electrolytic oxygen generation at the anode (Figure 3B). In the electrolytic mesocosm, at the start of the experiment the ORP was around 0 V vs. Ag/AgCl, then it gradually increased at all sampling points during the initial 120 days of operation, before stabilizing, or slightly decreasing during the remainder of the test. Specifically, at E1, the sediment redox potential reached a peak of +320 mV, after 77 days of operation (i.e., t1), whereas at E3 (i.e., positioned 30 cm apart from E1) and at E5 (positioned 60 cm apart from E1), the redox potential reached lower peak values of +310 V and +220 V, respectively, only after 135 days of operation. From day 120 onward, a slow decrease in the redox potential was observed at all sampling points. At the end of the study, however, the redox potential remained between +250 mV (at E1 and E3) and +150 mV (at E5).

A strikingly different trend was observed in the control mesocosm, whereby after a period of around 120 days during which the redox potential remained nearly stable at around 0 V, it gradually decreased down to -200 mV by the end of the study, suggesting the establishment of anoxic conditions, most likely driven by the metabolic activity of naturally-occurring sulfate reducing microorganisms.

Collectively, these results provide a clear indication that application of low-voltage direct current, prompting seawater electrolysis, allows increasing the redox potential of the sediment, thereby creating conditions that are potentially conducive for the aerobic biodegradation of oil hydrocarbons. Most importantly, the effect of electrolysis was apparent even at a distance of over 45 cm from the edge of the anode, and also in the presence of a continuous flow of seawater over the surface of the sediment.

3.2 GC-MS analysis of aromatic and aliphatic hydrocarbons

As far as the concentration of main oil components is concerned, Figure 4 shows the hopane-normalized concentration of C_0-C_4-alkylated PAHs (naphthalenes, fluorenes, dibenzothiophenes, pyrenes, and chrysenes) in the electrolytic mesocosm, at the different sampling times (t1, t2, t3) and locations (E1, E3, E5), relative to the individual t0 samples, measured in %.

Figure 4.

Although, experimental data appeared to be affected by a substantial variability, most likely caused by the intrinsic heterogeneity of the sediment material and uneven distribution contaminants, a time-dependent decrease in the content of nearly all PAHs and methylated PAHs was apparent in sediment samples taken just over the anode (i.e., sampling point E1), with removal efficiencies ranging from 80% to 100% at the last sampling time. Substantial, though incomplete, removal of PAHs was also observed in E3, located approximately 15 cm apart from the edge of the anode. By contrast, negligible removal of PAHs was observed in

samples taken at E5, with concentrations measured at the last sampling time (i.e., t3), in some cases even exceeding those detected at time zero (i.e., t0) (Figure 4).

As far as the Control experiment is concerned, negligible removal of PAHs was observed over time, at all sampling locations (Figure 5), with concentrations measured at the end of the study being typically equal or higher than those detected at t0. This latter finding provides a straightforward indication that the observed removal of PAHs in the electrolytic mesocosm was driven by the application of electric current.

Figure 5.

As far as the aliphatic hydrocarbons (nC_{13} to nC_{30}) are concerned, in the electrolytic mesocosm a time-dependent decrease in their concentrations (relative to t0) was observed almost exclusively at E1, whereas negligible changes were detected at further distance from the electrode (i.e., at E3 and E5) (Figure S1). Unexpectedly, the extent of removal of individual aliphatic hydrocarbons at E1 apparently increased with the length of the carbon chain, eventually reaching 45% in the case of nC_{30} (Figure S1).

In agreement with what observed in the case of PAHs, negligible removal of aliphatic hydrocarbons, irrespective of the chain length, was observed at all sampling locations in the control mesocosm (Figure S2), hence providing an additional line of evidence that the observed removal of hydrocarbons was triggered by the applied electric current.

3.3 Analysis of aromatic and aliphatic hydrocarbons with biosensors

Sediment samples from the electrolytic and the control mesocosms were also analyzed for target aromatic and aliphatic hydrocarbons by means of *ad hoc* developed biosensors. Besides

permitting the quantification of low molecular weight compounds that could not be analyzed via GC-MS (i.e., nC_6 to nC_{10} aliphatic hydrocarbons), biosensors also allowed an integral assessment of the progress of the bioremediation process from the quantification of lumped parameters (e.g., total PAHs). Figure 6A shows the normalized response of the biosensors for aliphatic compounds to samples taken from the electrolytic and the control mesocosms at different times (t0, t1, t2, t3). The biosensor targeting nC_6-nC_{10} indicated no apparent removal of hydrocarbons in the control mesocosm, with concentrations measured at the last sampling time (t3) being very similar or even higher than those measured at t0. A different situation was observed in the electrolytic mesocosm, with a consistent disappearance of contaminants being detected over time in the E1 sample and, though less clearly, also in sample E3. By contrast, negligible removal of nC_6-nC_{10} was observed in E5. As far as the biosensor for pristane is concerned (Figure 6B), no apparent removal was noticed both in the electrolytic and in the control mesocosm, in agreement with GC-MS data (data not shown).

Figure 6.

Figure 7 reports the results of the biosensors for aromatic hydrocarbons. Also in this case, in agreement with the results of oil chemistry obtained via GC-MS analysis, the biosensor detected a substantial time-dependent removal of aromatic hydrocarbons (i.e., BTX and PAH) in the electrolytic mesocosm only, and specifically in correspondence of E1, whereas lower to no-removal was detected at E3 and E5 and in the Control experiment.

Figure 7.

3.4 Diagnostic ratios and PAHs plots

In order to gain a deeper understanding of the prevalent oil hydrocarbons removal mechanisms (i.e., removal via electroosmosis vs. biodegradation), a number of key diagnostic ratios were calculated, from GC-MS oil chemistry analyses, for each sample and were normalized to the same ratio as measured in the original oil. Conventionally, it is assumed that, due to the different intrinsic biodegradability of the different oil components, the progress of biodegradation would result in a gradual decrease of these specific ratios. As an example, pristane (Pr) and phytane (Ph) are known to degrade at a slower rate compared to nC_{17} and nC_{18}. Therefore, it is expected that, upon biodegradation the specific ratios nC_{17}/Pr and nC_{18}/Ph would diminish over time. Same considerations apply for aromatic compounds. By contrast, removal mechanisms not linked to biodegradation, such as electroosmosis-driven mass transport, would proceed at comparable rates for compounds having similar structures such as nC_{17} and Pr and therefore, would not result in a net decrease of the corresponding diagnostic ratio. A detailed description of all diagnostic ratios herein calculated can be found elsewhere (Scheibye et al., 2017). For E1 samples, due to the extensive removal of most hydrocarbons, some diagnostic ratio became undetectable at the last sampling time (t3) (Figure S3). For some others, such as nC_{17}/Pr, and 2MN/1MN a little decrease (<10%) was observed over the course of the experiment (Figure S3). In the case of E3 and E5 samples, in which the extent of hydrocarbons removal was substantially lower than in E1 due to the greater distance from the anode, all diagnostic ratios could be calculated, and none displayed a substantial time-dependent reduction. Same considerations also apply to the control experiment, whereby all diagnostic ratios remained virtually unchanged over time. Taken as a whole, these findings suggest that, under the experimental conditions applied in this study, in the electrolytic mesocosm, removal of PAH and nC_{13}-nC_{30} was mainly due to electroosmosis rather than to biodegradation.

455 According to the Helmholtz-Smoluchowsky equation (Alshawabkeh et al., 1999; Cameselle
456 and Reddy, 2012), the electroosmotic flow from the anode to the overlying cathode was
457 estimated to be around 250 mL/d (assuming a coefficient of electroosmotic conductivity of
458 5×10^{-9} $m^2/ V s$). Taking into account that the herein used sediment was "freshly"
459 contaminated and therefore PAH were only loosely bound to the sediment material, it is
460 plausible that in the presence of such a relatively high electroosmotic flow, the electrokinetic
461 transport proceeded at substantially higher rates compared to aerobic biodegradation.
462 Possibly, a different scenario could be expected in the case of "historically" contaminated
463 sediments and/or in the presence of a more active indigenous hydrocarbonoclastic microbial
464 community.
465 By contrast, with specific reference to lower MW alkanes, biosensor analyses indicated a
466 remarkable reduction in their concentration levels which was not mirrored by a
467 corresponding reduction in the concentration level of pristane. Therefore, under the
468 assumption that the physico-chemical behavior of nC_6 to nC_{10} is somewhat similar to that of
469 pristane, it seems likely that biodegradation was the primary removal mechanism for such oil
470 components, although further lines of evidence are warranted.
471 The finding that electroosmosis was less effective in removing aliphatics with respect to PAHs
472 is a somewhat unexpected finding that, however, could be related to their lower affinity for
473 water (i.e., higher octanol/water partition coefficient). Being less prone to be removed via
474 electroosmosis, these contaminants remained within the tanks for longer period of times.
475 Under such conditions, aerobic biodegradation apparently assumed a more relevant role,
476 especially in the case of low molecular weight alkanes (i.e., nC_6 to nC_{10}),
477

3.5 Microbiological analyses (Next Generation Sequencing and CARD-FISH detection of alkB-gene carrying cells)

Sediment samples taken at different times (t0 to t2) and positions (E1 to E5 and C1 to C5) from the electrolytic and control mesocosms were also analyzed by next-generation sequencing for identifying the dynamics of the main microbial community members, as well as, their spatial distribution (Figures 8, 9 and S5).

Figure 8.

Bray-Curtis similarities were calculated from 16S rRNA gene sequencing profiles and non-metric multidimensional scaling (nMDS) was used to assess changes in the microbial communities in electrolytic and control mesocosms (Figure 8). At time 0, microbial communities in the electrolytic mesocosm were distinct from those in the control mesocosm (Figure 8, triangles). This finding is not surprising taking into account the substantial heterogeneity of the sediment samples as also confirmed by previously described oil hydrocarbon analyses. However, within the distinct clusters, there was high similarity between sediment communities at all locations (i.e. situated close to the anode (E1) or further from the anode (E5)), and also between replicate samples (≥60-80% similarity, Figure 8). Interestingly, microbial community compositions converged at t1 (i.e., day 77) in electrolytic (E5) and control (C1) (Figure 8) with a high relative abundance of known aerobic hydrocarbon degraders, *Alcanivorax* and *Marinobacter*, in both systems (Figure 9A, B). There were successional changes in the microbial communities over time, with marked differences between t1 and t2 electrolytic and control mesocosms. Furthermore, at t2 (i.e., day 135) there appeared to be a zone of influence surrounding the anode as shown by distinct differences in the microbial communities with increasing distance from the anode in the electrified system

(Figure 8, circles). The five most abundant phyla in the electrolytic mesocosms were *Gammaproteobacteria* (56.1% ±8.3), *Alphaproteobacteria* (10.5% ±1.4), *Bacteroidetes* (12.9% ±3.8), *Firmicutes* (7.6% ±4.9) and *Deltaproteobacteria* (3.3% ±1.1) (Figure S5). Generally, the same phyla were detected in the electrolytic and control mesocosms, however there were differences in the relative abundance of the different phyla, with a marked increase in *Deltaproteobacteria* at C5 after 135 days (Figure S5) which coincided with a decrease in redox and the establishment of anoxic conditions in the control mesocosm (Figure 3). Following a more detailed analysis of the microbial communities, an increasing relative abundance of anaerobic, thermophilic spore-forming microbes within class *Clostridia* were detected over time in the microbial communities surrounding the anode (e.g., *Thermovenabulum, Desulfotomaculum, Sporotomaculum,* E1, Figure 9C), compared to communities observed in the control mesocosm and sites situated further from the anode (C1, E3, E5 at t0, t1, t2 ≤0.0005 ±0.0002 % rel. abundance). Sulfate-reducing *Desulfotomaculum* spp. have previously been isolated from oil fields and are implicated in oil biodegradation (Guan et al., 2013; Lan et al., 2011; Leu et al., 1998; Liu et al., 2008; Rosnes et al., 1991).

Figure 9.

As far as the CARD-FISH detection and quantification of the alkB gene is concerned, experimental data revealed a remarkable time-dependent increase in the concentration of *Alcanivorax borkumensis* carrying the alkB-gene in the electrolytic mesocosm at E1 and, though to a lesser extent, also at E5, hence confirming the beneficial role of electrolysis in the stimulation of aerobic hydrocarbonoclastic communities (Figure 10). In the control experiment a small increase was noticed only at C5. Taken as a whole microbiological data

provided an additional line of evidence to previously mentioned biosensors data of the stimulatory effect of electrolysis on biodegradation of (low molecular weight) alkanes.

Figure 10.

Long-term durability of electrode materials

At the end of the 230-day experimental period, the electrodes were removed from the electrolytic mesocosm and visually examined in order to assess their structural integrity. Apparently, the integrity of the Ti-mesh anode was fully preserved (Figure 11), whereas the stainless-steel cathode appeared to be highly deteriorated with evident pitting corrosion. This finding has important economic implications, particularly in consideration of the fact that the cost of used anode material (approx. 1000€/m^2) is orders of magnitude higher than that of the stainless-steel cathode. Clearly, further studies, also involving detailed microscopic and electrochemical analyses, would be warranted to more precisely assess the impact of "aging" of electrodes on their (bio)electrochemical performance.

Figure 11.

4. Conclusive remarks

The main results of this mesocosm-scale electrobioremediation study can be summarized as follows:

- Electrobioremediation proved to be a sustainable technology to remove hydrocarbons, particularly PAHs, from contaminated sediments, being characterized by a low energy footprint and a negligible need of maintenance.

- Electrobioremediation increased the ORP of the sediment, via oxygen generation, even at distance of 60 cm from the edge of the anode, despite the low applied current density of around 10 A/m^2 and resulting electric power consumption of 2.25 W.
- Consistent with electrolytic oxygen generation, electrobioremediation resulted in a remarkable increase in the concentration of *Alcanivorax borkumensis* cells (i.e., a known aerobic hydrocarbonoclastic bacterium) carrying the alkB-gene and in the development of specialized microbial communities, as determined by NGS analysis.
- Both electroosmosis and biodegradation (though to this latter to a lesser extent) contributed to the removal of contaminants from the sediment, with their relative contribution being highly dependent on the nature of contaminants.
- Further work is warranted to identify optimal operational strategies of the electrobioremediation system which allow to synergistically exploit the contribution electrokinetic and biodegradation processes to the removal of petroleum hydrocarbons from contaminated sites, since these two mechanisms appear to be a complex function of a high number of variables including type and levels of contaminants, activity of naturally occurring microbial community and applied electrochemical conditions (e.g., current density).

Acknowledgements

This work was financially supported by the European Commission within the Seventh Framework Programme under Grant Agreement No. 312139 ("Kill-Spill: Integrated biotechnological solutions for combating marine oil spills").

References

Abril, M.A., Michan, C., Timmis, K.N., Ramos, J.L., 1989. Regulator and enzyme specificities of the TOL plasmid-encoded upper pathway for degradation of aromatic hydrocarbons and

580 expansion of the substrate range of the pathway. J. Bacteriol. 171, 6782–90.

581 Acar, Y.B., Alshawabkeh, A.N., 1993. Principles of electrokinetic remediation. Environ. Sci.
582 Technol. 27, 2638–2647. doi:10.1021/es00049a002

583 Acar, Y.B., Gale, R.J., Alshawabkeh, A.N., Marks, R.E., Puppala, S., Bricka, M., Parker, R., 1995.
584 Electrokinetic remediation: Basics and technology status. J. Hazard. Mater. 40, 117–137.
585 doi:10.1016/0304-3894(94)00066-P

586 Alshawabkeh, A.N., Yeung, A.T., Bricka, M.R., 1999. Practical Aspects of In-Situ Electrokinetic
587 Extraction. J. Environ. Eng. doi:10.1061/(ASCE)0733-9372(1999)125:1(27)

588 Atlas, R.M., Bartha, R., 1972. Degradation Atlas, R.M., Bartha, R., 1972. Degradation and
589 mineralization of petroleum in sea water: Limitation by nitrogen and phosphorous.
590 Biotechnol. Bioeng. 14, 309–318. doi:10.1002/bit.260140304and mineralization of
591 petroleum in sea water: Limitation. Biotechnol. Bioeng. 14, 309–318.
592 doi:10.1002/bit.260140304

593 Aulenta, F., Canosa, A., Reale, P., Rossetti, S., Panero, S., Majone, M., 2009. Microbial reductive
594 dechlorination of trichloroethene to ethene with electrodes serving as electron donors
595 without the external addition of redox mediators. Biotechnol. Bioeng. 103, 85–91.
596 doi:10.1002/bit.22234

597 Barba, S., López-Vizcaíno, R., Saez, C., Villaseñor, J., Cañizares, P., Navarro, V., Rodrigo, M.A.,
598 2018. Electro-bioremediation at the prototype scale: What it should be learned for the
599 scale-up. Chem. Eng. J. 334, 2030–2038. doi:10.1016/j.cej.2017.11.172

600 Barra Caracciolo, A., Grenni, P., Cupo, C., Rossetti, S., 2005. In situ analysis of native microbial
601 communities in complex samples with high particulate loads. FEMS Microbiol. Lett. 253,
602 55–58. doi:10.1016/j.femsle.2005.09.018

603 Bellagamba, M., Cruz Viggi, C., Ademollo, N., Rossetti, S., Aulenta, F., 2017. Electrolysis-driven
604 bioremediation of crude oil-contaminated marine sediments. N. Biotechnol. 38.
605 doi:10.1016/j.nbt.2016.03.003

606 Boopathy, R., 2017. Anaerobic Degradation of Petroleum Hydrocarbons in Sediments, in:
607 Current Developments in Biotechnology and Bioengineering. Elsevier, pp. 475–490.
608 doi:10.1016/B978-0-444-63664-5.00020-4

609 Boufadel, M.C., Reeser, P., Suidan, M.T., Wrenn, B.A., Cheng, J., Du, X., Huang, T.L., Venosa, A.D.,
610 1999. Optimal Nitrate Concentration for the Biodegradation of n-Heptadecane in a
611 Variably-Saturated Sand Column. Environ. Technol. 20, 191–199.
612 doi:10.1080/09593332008616808

613 Bray, J.R., Curtis, J.T., 1957. An Ordination of the Upland Forest Communities of Southern
614 Wisconsin. Ecol. Monogr. 27, 325–349. doi:10.2307/1942268

615 Cameselle, C., Reddy, K.R., 2012. Development and enhancement of electro-osmotic flow for
616 the removal of contaminants from soils. Electrochim. Acta 86, 10–22.
617 doi:10.1016/j.electacta.2012.06.121

618 Caporaso, J.G., Bittinger, K., Bushman, F.D., DeSantis, T.Z., Andersen, G.L., Knight, R., 2010a.
619 PyNAST: a flexible tool for aligning sequences to a template alignment. Bioinformatics 26,
620 266–267. doi:10.1093/bioinformatics/btp636

621 Caporaso, J.G., Kuczynski, J., Stombaugh, J., Bittinger, K., Bushman, F.D., Costello, E.K., Fierer, N.,
622 Peña, A.G., Goodrich, J.K., Gordon, J.I., Huttley, G.A., Kelley, S.T., Knights, D., Koenig, J.E.,
623 Ley, R.E., Lozupone, C.A., McDonald, D., Muegge, B.D., Pirrung, M., Reeder, J., Sevinsky, J.R.,
624 Turnbaugh, P.J., Walters, W.A., Widmann, J., Yatsunenko, T., Zaneveld, J., Knight, R., 2010b.
625 QIIME allows analysis of high-throughput community sequencing data. Nat. Methods 7,
626 335–336. doi:10.1038/nmeth.f.303

627 Chanton, J., Zhao, T., Rosenheim, B.E., Joye, S., Bosman, S., Brunner, C., Yeager, K.M., Diercks,
628 A.R., Hollander, D., 2015. Using Natural Abundance Radiocarbon To Trace the Flux of
629 Petrocarbon to the Seafloor Following the Deepwater Horizon Oil Spill. Environ. Sci.
630 Technol. 49, 847–854. doi:10.1021/es5046524

631 Clarke, K.R., Gorley, R.N., 2015. PRIMER v7: User Manual/Tutorial. PRIMER-E, Plymouth.

632 Cruz Viggi, C., Presta, E., Bellagamba, M., Kaciulis, S., Balijepalli, S.K., Zanaroli, G., Petrangeli
633 Papini, M., Rossetti, S., Aulenta, F., 2015. The "Oil-Spill Snorkel": an innovative
634 bioelectrochemical approach to accelerate hydrocarbons biodegradation in marine
635 sediments. Front. Microbiol. 6. doi:10.3389/fmicb.2015.00881

636 da Cruz, G.F., de Vasconcellos, S.P., Angolini, C.F., Dellagnezze, B.M., Garcia, I.N., de Oliveira,
637 V.M., dos Santos Neto, E. V, Marsaioli, A.J., 2011. Could petroleum biodegradation be a
638 joint achievement of aerobic and anaerobic microrganisms in deep sea reservoirs? AMB
639 Express 1, 47. doi:10.1186/2191-0855-1-47

640 Daghio, M., Espinoza Tofalos, A., Leoni, B., Cristiani, P., Papacchini, M., Jalilnejad, E., Bestetti, G.,
641 Franzetti, A., 2018. Bioelectrochemical BTEX removal at different voltages: assessment of
642 the degradation and characterization of the microbial communities. J. Hazard. Mater. 341,
643 120–127. doi:10.1016/j.jhazmat.2017.07.054

644 Daghio, M., Vaiopoulou, E., Patil, S.A., Suárez-Suárez, A., Head, I.M., Franzetti, A., Rabaey, K.,
645 2016. Anodes Stimulate Anaerobic Toluene Degradation via Sulfur Cycling in Marine
646 Sediments. Appl. Environ. Microbiol. 82, 297–307. doi:10.1128/AEM.02250-15

647 Daly, K.L., Passow, U., Chanton, J., Hollander, D., 2016. Assessing the impacts of oil-associated
648 marine snow formation and sedimentation during and after the Deepwater Horizon oil
649 spill. Anthropocene 13, 18–33. doi:10.1016/j.ancene.2016.01.006

650 DeSantis, T.Z., Hugenholtz, P., Larsen, N., Rojas, M., Brodie, E.L., Keller, K., Huber, T., Dalevi, D.,
651 Hu, P., Andersen, G.L., 2006. Greengenes, a Chimera-Checked 16S rRNA Gene Database
652 and Workbench Compatible with ARB. Appl. Environ. Microbiol. 72, 5069–5072.
653 doi:10.1128/AEM.03006-05

654 Domínguez-Garay, A., Quejigo, J.R., Dörfler, U., Schroll, R., Esteve-Núñez, A., 2018.
655 Bioelectroventing: an electrochemical-assisted bioremediation strategy for cleaning-up
656 atrazine-polluted soils. Microb. Biotechnol. 11, 50–62. doi:10.1111/1751-7915.12687

657 Dyksterhouse, S.E., Gray, J.P., Herwig, R.P., Lara, J.C., Staley, J.T., 1995. Cycloclasticus pugetii
658 gen. nov., sp. nov., an Aromatic hydrocarbon- degrading bacterium from marine
659 sediments 45, 116–123.

660 Edgar, R.C., 2010. Search and clustering orders of magnitude faster than BLAST.
661 Bioinformatics 26, 2460–2461. doi:10.1093/bioinformatics/btq461

662 Gallotta, F.D.C., Christensen, J.H., 2012. Source identification of petroleum hydrocarbons in soil
663 and sediments from Iguaçu River Watershed, Paraná, Brazil using the CHEMSIC method
664 (CHEMometric analysis of Selected Ion Chromatograms). J. Chromatogr. A 1235, 149–
665 158. doi:10.1016/J.CHROMA.2012.02.041

666 Gong, Y., Zhao, X., Cai, Z., O'Reilly, S.E., Hao, X., Zhao, D., 2014. A review of oil, dispersed oil and
667 sediment interactions in the aquatic environment: Influence on the fate, transport and
668 remediation of oil spills. Mar. Pollut. Bull. 79, 16–33.
669 doi:10.1016/j.marpolbul.2013.12.024

670 Guan, J., Xia, L.-P., Wang, L.-Y., Liu, J.-F., Mu, B.-Z., 2013. Diversity and distribution of sulfate-
671 reducing bacteria in four petroleum reservoirs detected by using 16S rRNA and dsrAB
672 genes. Int. Biodeterior. Biodegradation 76, 58–66. doi:10.1016/J.IBIOD.2012.06.021

673 Haas, B.J., Gevers, D., Earl, A.M., Feldgarden, M., Ward, D. V., Giannoukos, G., Ciulla, D., Tabbaa,
674 D., Highlander, S.K., Sodergren, E., Methe, B., DeSantis, T.Z., Petrosino, J.F., Knight, R.,
675 Birren, B.W., 2011. Chimeric 16S rRNA sequence formation and detection in Sanger and
676 454-pyrosequenced PCR amplicons. Genome Res. 21, 494–504.
677 doi:10.1101/gr.112730.110

678 Hernández-Sánchez, V., Molina, L., Ramos, J.L., Segura, A., 2016. New family of biosensors for
679 monitoring BTX in aquatic and edaphic environments. Microb. Biotechnol. 9, 858–867.
680 doi:10.1111/1751-7915.12394

681 Kronenberg, M., Trably, E., Bernet, N., Patureau, D., 2017. Biodegradation of polycyclic
682 aromatic hydrocarbons: Using microbial bioelectrochemical systems to overcome an
683 impasse. Environ. Pollut. 231, 509–523. doi:10.1016/j.envpol.2017.08.048

684 Kuppusamy, S., Thavamani, P., Venkateswarlu, K., Lee, Y.B., Naidu, R., Megharaj, M., 2017.
685 Remediation approaches for polycyclic aromatic hydrocarbons (PAHs) contaminated
686 soils: Technological constraints, emerging trends and future directions. Chemosphere
687 168, 944–968. doi:10.1016/j.chemosphere.2016.10.115

688 Lan, G., Li, Z., Zhang, H., Zou, C., Qiao, D., Cao, Y., 2011. Enrichment and diversity analysis of the
689 thermophilic microbes in a high temperature petroleum reservoir. African J. Microbiol.
690 Res. 5, 1850–1857. doi:10.5897/AJMR11.354

691 Leu, J.-Y., McGovern-Traa, C.P., Porter, A.J.., Harris, W.J., Hamilton, W.A., 1998. Identification
692 and Phylogenetic Analysis of Thermophilic Sulfate-Reducing Bacteria in Oil Field Samples
693 by 16S rDNA Gene Cloning and Sequencing. Anaerobe 4, 165–174.
694 doi:10.1006/anae.1998.0156

695 Li, X., Wang, X., Ren, Z.J., Zhang, Y., Li, N., Zhou, Q., 2015. Sand amendment enhances
696 bioelectrochemical remediation of petroleum hydrocarbon contaminated soil.

Chemosphere 141, 62–70. doi:10.1016/j.chemosphere.2015.06.025

Lim, M.W., Lau, E. Von, Poh, P.E., 2016. A comprehensive guide of remediation technologies for oil contaminated soil — Present works and future directions. Mar. Pollut. Bull. 109, 14–45. doi:10.1016/j.marpolbul.2016.04.023

Lim, S.K., Shin, H.S., Yoon, K.S., Kwack, S.J., Um, Y.M., Hyeon, J.H., Kwak, H.M., Kim, J.Y., Kim, T.H., Kim, Y.J., Roh, T.H., Lim, D.S., Shin, M.K., Choi, S.M., Kim, H.S., Lee, B.-M., 2014. Risk Assessment of Volatile Organic Compounds Benzene, Toluene, Ethylbenzene, and Xylene (BTEX) in Consumer Products. J. Toxicol. Environ. Heal. Part A 77, 1502–1521. doi:10.1080/15287394.2014.955905

Liu, Y., Nikolausz, M., Jin, P., 2008. Abundance and diversity of sulphate-reducing bacteria within a crude oil gathering and transferring system in China. Ann. Microbiol. 58, 611–615. doi:10.1007/BF03175565

Luo, Q., Zhang, X., Wang, H., Qian, Y., 2005. Mobilization of phenol and dichlorophenol in unsaturated soils by non-uniform electrokinetics. Chemosphere 59, 1289–1298. doi:10.1016/j.chemosphere.2004.11.043

Mao, D., Lu, L., Revil, A., Zuo, Y., Hinton, J., Ren, Z.J., 2016. Geophysical Monitoring of Hydrocarbon-Contaminated Soils Remediated with a Bioelectrochemical System. Environ. Sci. Technol. 50, 8205–8213. doi:10.1021/acs.est.6b00535

Mapelli, F., Scoma, A., Michoud, G., Aulenta, F., Boon, N., Borin, S., Kalogerakis, N., Daffonchio, D., 2017. Biotechnologies for Marine Oil Spill Cleanup: Indissoluble Ties with Microorganisms. Trends Biotechnol. 35. doi:10.1016/j.tibtech.2017.04.003

Matturro, B., Frascadore, E., Cappello, S., Genovese, M., Rossetti, S., 2016. In situ detection of alkB2 gene involved in Alcanivorax borkumensis SK2 T hydrocarbon biodegradation.

720 Mar. Pollut. Bull. 110, 378–382. doi:10.1016/j.marpolbul.2016.06.038

721 Modin, O., Aulenta, F., 2017. Three promising applications of microbial electrochemistry for
722 the water sector. Environ. Sci. Water Res. Technol. 3. doi:10.1039/c6ew00325g

723 Mosmeri, H., Tasharrofi, S., Alaie, E., Sadegh Hassani, S., 2018. Controlled-release oxygen
724 nanocomposite for bioremediation of benzene contaminated groundwater, in: New
725 Polymer Nanocomposites for Environmental Remediation. Elsevier, pp. 601–622.
726 doi:10.1016/B978-0-12-811033-1.00023-8

727 Passow, U., Sweet, J., Quigg, A., 2017. How the dispersant Corexit impacts the formation of
728 sinking marine oil snow. Mar. Pollut. Bull. 125, 139–145.
729 doi:10.1016/j.marpolbul.2017.08.015

730 Rakoczy, J., Feisthauer, S., Wasmund, K., Bombach, P., Neu, T.R., Vogt, C., Richnow, H.H., 2013.
731 Benzene and sulfide removal from groundwater treated in a microbial fuel cell.
732 Biotechnol. Bioeng. 110, 3104–3113. doi:10.1002/bit.24979

733 Rodrigo Quejigo, J., Dörfler, U., Schroll, R., Esteve-Núñez, A., 2016. Stimulating soil
734 microorganisms for mineralizing the herbicide isoproturon by means of microbial
735 electroremediating cells. Microb. Biotechnol. 9, 369–380. doi:10.1111/1751-7915.12351

736 Romero, I.C., Toro-Farmer, G., Diercks, A.-R., Schwing, P., Muller-Karger, F., Murawski, S.,
737 Hollander, D.J., 2017. Large-scale deposition of weathered oil in the Gulf of Mexico
738 following a deep-water oil spill. Environ. Pollut. 228, 179–189.
739 doi:10.1016/j.envpol.2017.05.019

740 Rosnes, J.T., Torsvik, T., Lien, T., 1991. Spore-forming thermophilic sulfate-reducing bacteria
741 isolated from north sea oil field waters. Appl. Environ. Microbiol. 57, 2302–7.

742 Salminen, J.M., Tuomi, P.M., Suortti, A.-M., Jørgensen, K.S., 2004. Potential for Aerobic and

743 Anaerobic Biodegradation of Petroleum Hydrocarbons in Boreal Subsurface.
744 Biodegradation 15, 29–39. doi:10.1023/B:BIOD.0000009954.21526.e8

745 Scheibye, K., Christensen, J.H., Johnsen, A.R., 2017. Biodegradation of crude oil in Arctic
746 subsurface water from the Disko Bay (Greenland) is limited. Environ. Pollut. 223, 73–80.
747 doi:10.1016/J.ENVPOL.2016.12.032

748 Segura, A., Hernández-Sánchez, V., Marqués, S., Molina, L., 2017. Insights in the regulation of
749 the degradation of PAHs in Novosphingobium sp. HR1a and utilization of this regulatory
750 system as a tool for the detection of PAHs. Sci. Total Environ. 590–591, 381–393.
751 doi:10.1016/j.scitotenv.2017.02.180

752 Sevilla, E., Yuste, L., Moreno, R., Rojo, F., 2017. Differential expression of the three *Alcanivorax*
753 *borkumensis* SK2 genes coding for the P450 cytochromes involved in the assimilation of
754 hydrocarbons. Environ. Microbiol. Rep. 9, 797–808. doi:10.1111/1758-2229.12598

755 Sevilla, E., Yuste, L., Rojo, F., 2015. Marine hydrocarbonoclastic bacteria as whole-cell
756 biosensors for *n* -alkanes. Microb. Biotechnol. 8, 693–706. doi:10.1111/1751-
757 7915.12286

758 Singh, A.K., Sherry, A., Gray, N.D., Jones, D.M., Bowler, B.F.J., Head, I.M., 2014. Kinetic
759 parameters for nutrient enhanced crude oil biodegradation in intertidal marine
760 sediments. Front. Microbiol. 5. doi:10.3389/fmicb.2014.00160

761 Stout, S.A., German, C.R., 2018. Characterization and flux of marine oil snow settling toward
762 the seafloor in the northern Gulf of Mexico during the Deepwater Horizon incident:
763 Evidence for input from surface oil and impact on shallow shelf sediments. Mar. Pollut.
764 Bull. 129, 695–713. doi:10.1016/j.marpolbul.2017.10.059

765 Valentine, D.L., Fisher, G.B., Bagby, S.C., Nelson, R.K., Reddy, C.M., Sylva, S.P., Woo, M.A., 2014.

766 Fallout plume of submerged oil from *Deepwater Horizon*. Proc. Natl. Acad. Sci. 111,
767 15906–15911. doi:10.1073/pnas.1414873111

768 Wang, H., Luo, H., Fallgren, P.H., Jin, S., Ren, Z.J., 2015. Bioelectrochemical system platform for
769 sustainable environmental remediation and energy generation. Biotechnol. Adv. 33, 317–
770 334. doi:10.1016/j.biotechadv.2015.04.003

771 Wang, Q., Garrity, G.M., Tiedje, J.M., Cole, J.R., 2007. Naive Bayesian Classifier for Rapid
772 Assignment of rRNA Sequences into the New Bacterial Taxonomy. Appl. Environ.
773 Microbiol. 73, 5261–5267. doi:10.1128/AEM.00062-07

774 Wu, H., Sun, L., Wang, H., Wang, X., 2018. *In situ* sodium persulfate/calcium peroxide oxidation
775 in remediation of TPH-contaminated soil in 3D-sand box. Environ. Technol. 39, 91–101.
776 doi:10.1080/09593330.2017.1296029

777 Yan, F., Chen, W., Reible, D., 2015. Electrochemical Stimulation of PAH Biodegradation in
778 Sediment. Soil Sediment Contam. An Int. J. 24, 143–156.
779 doi:10.1080/15320383.2014.922932

780 Yan, F., Reible, D., 2015. Electro-bioremediation of contaminated sediment by electrode
781 enhanced capping. J. Environ. Manage. 155, 154–161.
782 doi:10.1016/j.jenvman.2015.03.023

783 Yan, F., Reible, D.D., 2012. PAH degradation and redox control in an electrode enhanced
784 sediment cap. J. Chem. Technol. Biotechnol. 87, 1222–1228. doi:10.1002/jctb.3767

785 Zhang, T., Gannon, S.M., Nevin, K.P., Franks, A.E., Lovley, D.R., 2010. Stimulating the anaerobic
786 degradation of aromatic hydrocarbons in contaminated sediments by providing an
787 electrode as the electron acceptor. Environ. Microbiol. 12, 1011–1020.
788 doi:10.1111/j.1462-2920.2009.02145.x

789 Zhao, X., Gong, Y., O'Reilly, S.E., Zhao, D., 2015. Effects of oil dispersant on solubilization,
790 sorption and desorption of polycyclic aromatic hydrocarbons in sediment–seawater
791 systems. Mar. Pollut. Bull. 92, 160–169. doi:10.1016/j.marpolbul.2014.12.042

792

793

Figure legends

Figure 1. (A) Schematic representation of the mesocosm-scale electrobioremediation experiment. (B) Picture of the two mesocosms positioned one next to the other within the larger tank, kept under a continuous-flow of seawater. Picture taken during the initial filling of the larger tank.

Figure 2. Schematic representation of the two mesocosms with indication of the sampling positions. The direction of seawater flow is from E1/C1 to E5/C5, as depicted in Figure 1B.

Figure 3. (A) Current and cell voltage throughout the whole experimental period for the electrolytic mesocosm. t0= day 0; t1 =day 77; t2 = day 135; t3 = day 230. (B) Time course of the sediment redox potential in the electrolytic and in the control mesocosms.

Figure 4. Hopane-normalized concentration of C_0-C_4-alkylated PAHs in the electrolytic mesocosm, at the different sampling times (t1, t2, t3), and points (E1, E3, E5) relative to t0 samples, measured in %. Note that columns marked with asterisks are above 150% of t0.

Figure 5. Hopane-normalized concentration of C_0-C_4-alkylated PAHs in the Control experiment, at the different sampling times (t1, t2, t3), and points (C1, C3, C5) relative to the average of all t0 samples, measured in %. Note that columns marked with asterisks are above 150% of t0.

Figure 6. Response of the biosensors for (A) nC_6 to nC_{10} and (B) pristane. A fluorescence induction higher than 2-fold (red dashed line in the graphs) was considered as indicative of the presence of hydrocarbons.

Figure 7. Response of the biosensors for (A) BTX and (B) PAHs. A fluorescence induction higher than 2-fold (red dashed line in the graphs) was considered as indicative of the presence of hydrocarbons.

Figure 8. Non-metric multidimensional scaling (nMDS) of Bray-Curtis similarities of 16S rRNA gene sequencing profiles from electrolytic (E) and control (C) mesocosms. Microbial community profiles were generated at t0, 77 days (t1) and 135 days (t2) at different distances from the anode (e.g. E1, E3, E5).

Figure 9. Putative hydrocarbon-degrading microbial communities in electrolytic and control mesocosms. Relative abundance (%) of aerobic hydrocarbon degraders across all treatments (A, B) and anaerobic, thermophilic spore-formers in E1 only (C).

Figure 10. Concentration of cells carrying the alkB-gene in samples from the electrolytic and the control mesocosm.

Figure 11. Appearance of the Ti-MMO anode and the Stainless-steel cathode at the start (A, C) and at the end (B, D) of the study.

Figure 1

Click here to download high resolution image

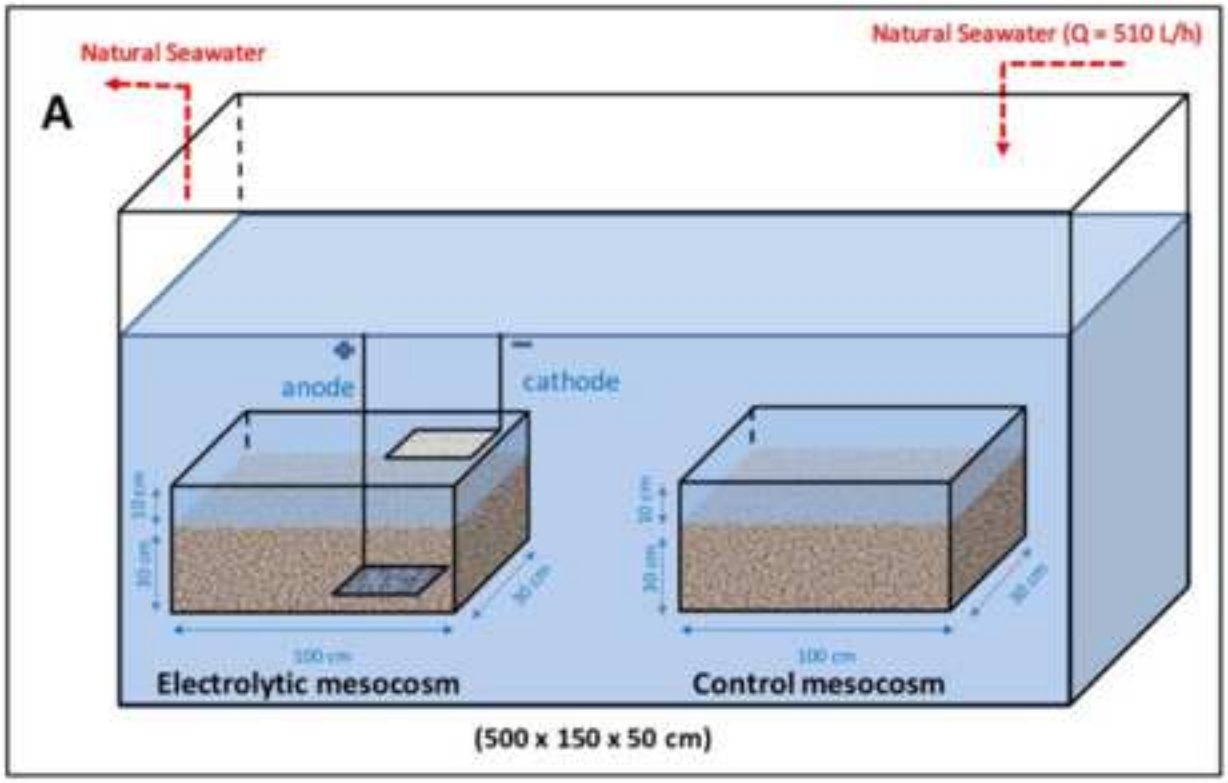

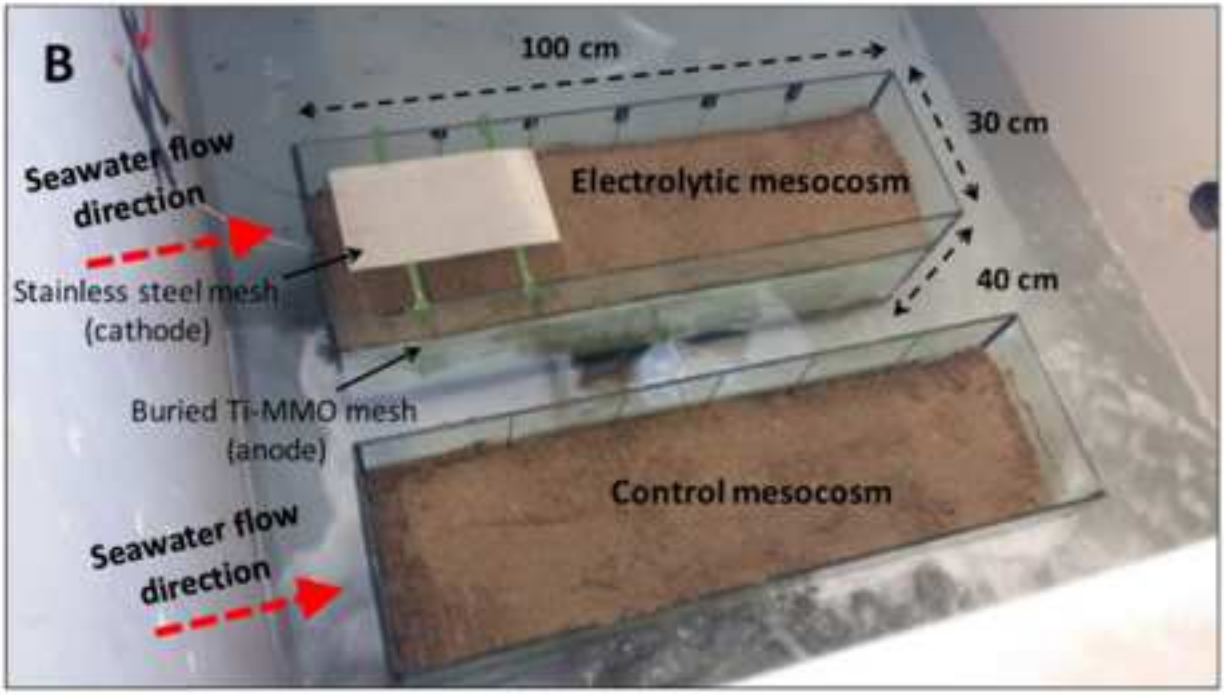

Figure 2

Click here to download high resolution image

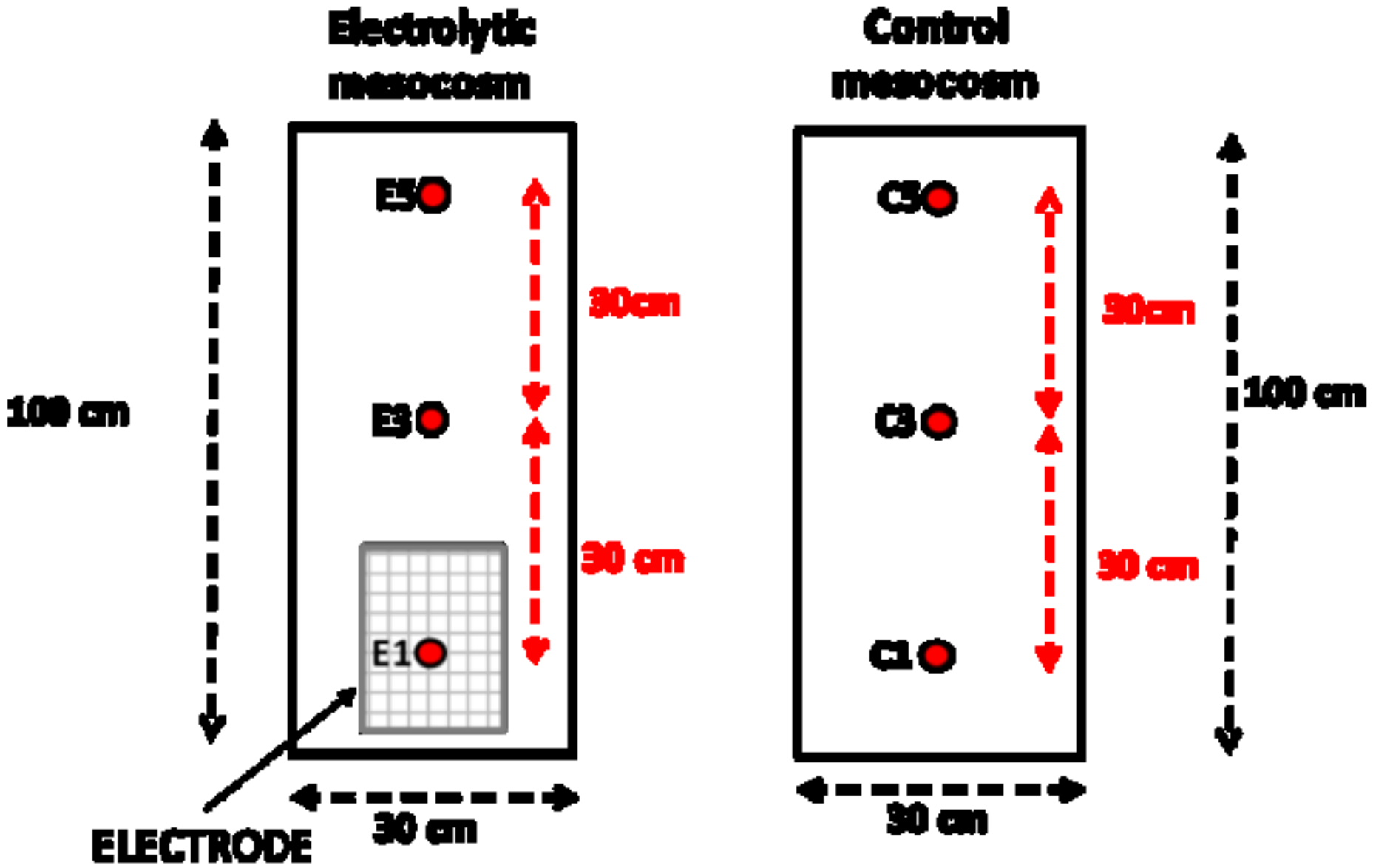

Figure 3

Click here to download high resolution image

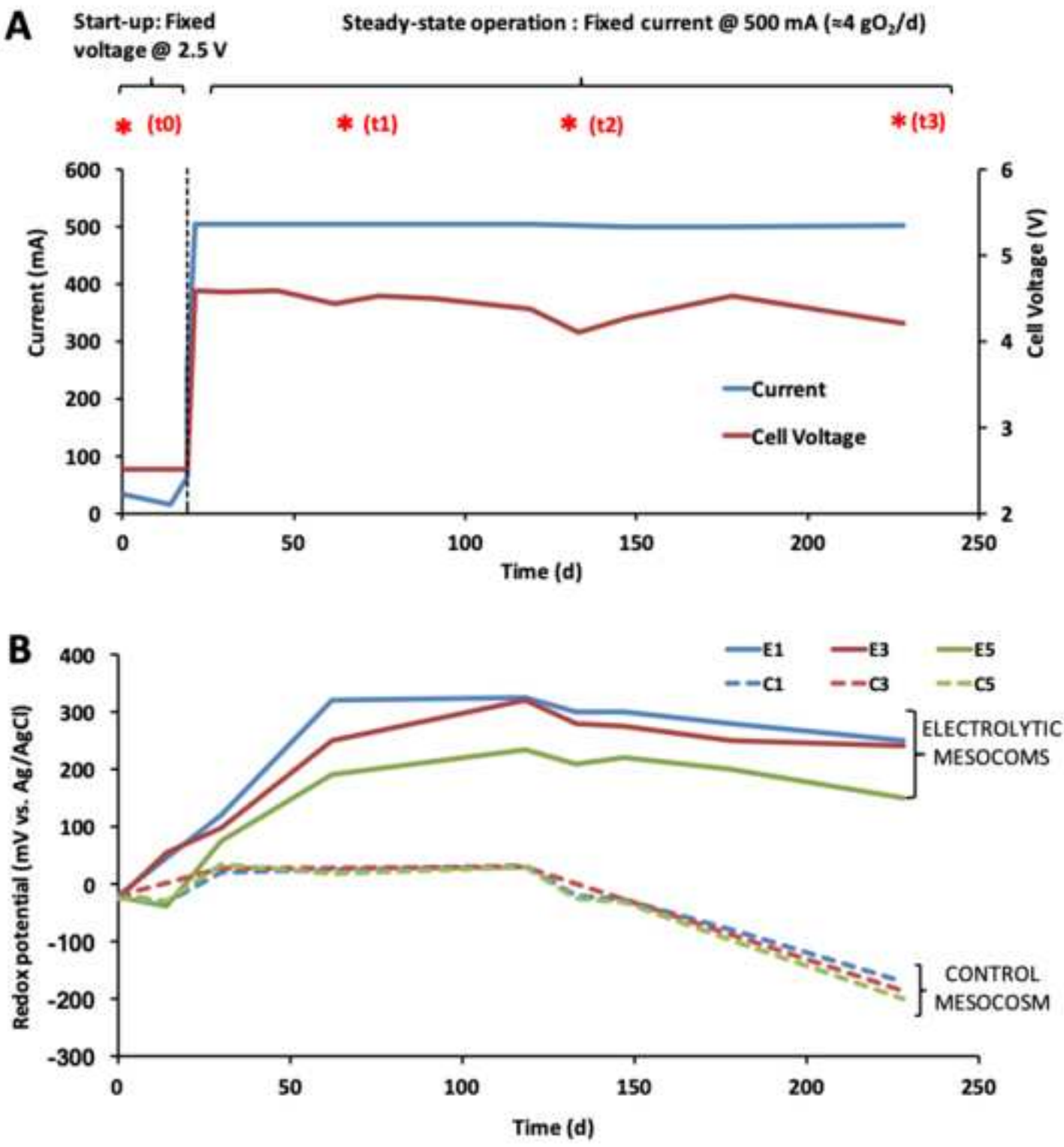

Figure 4

Click here to download high resolution image

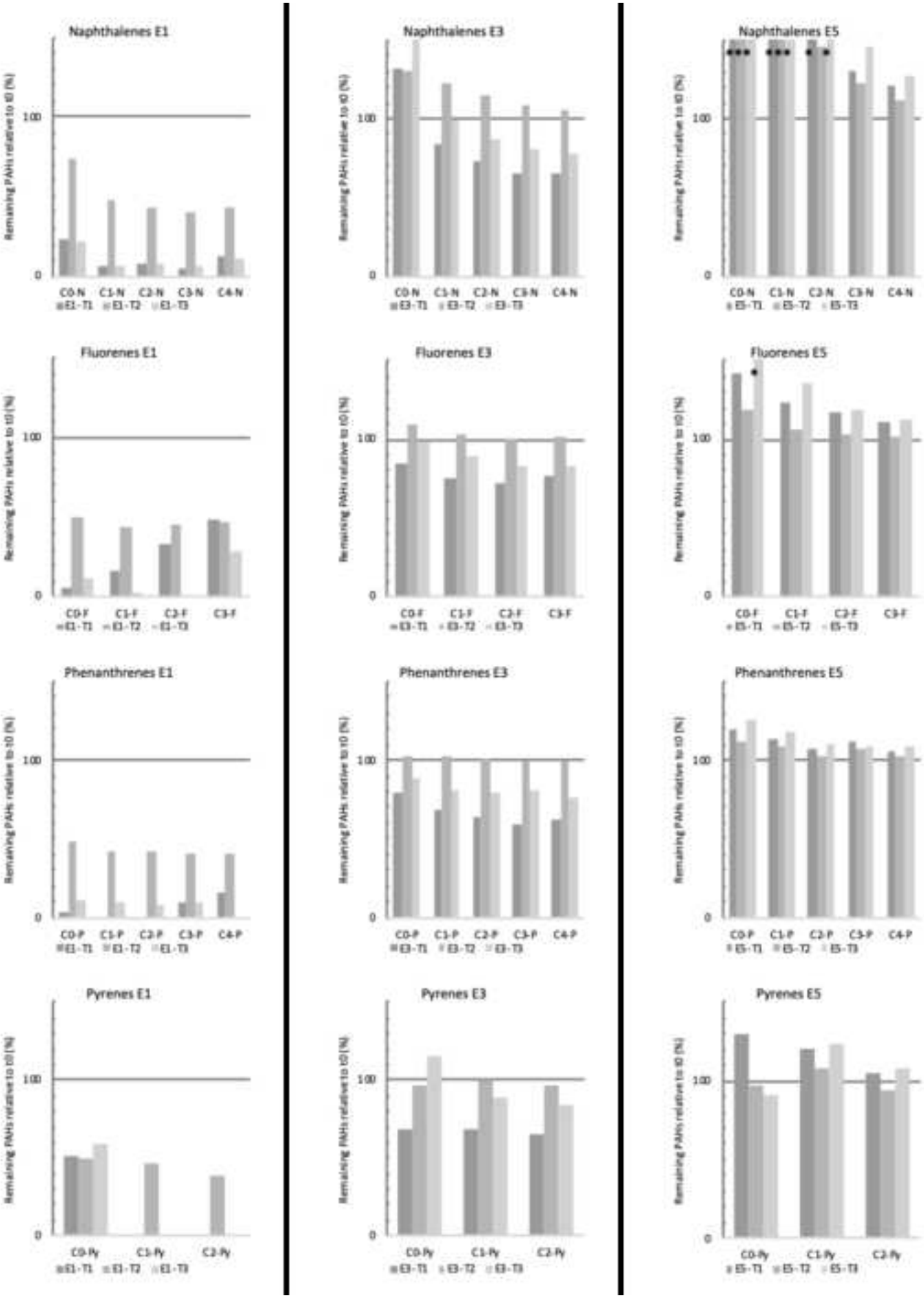

Figure 5

Click here to download high resolution image

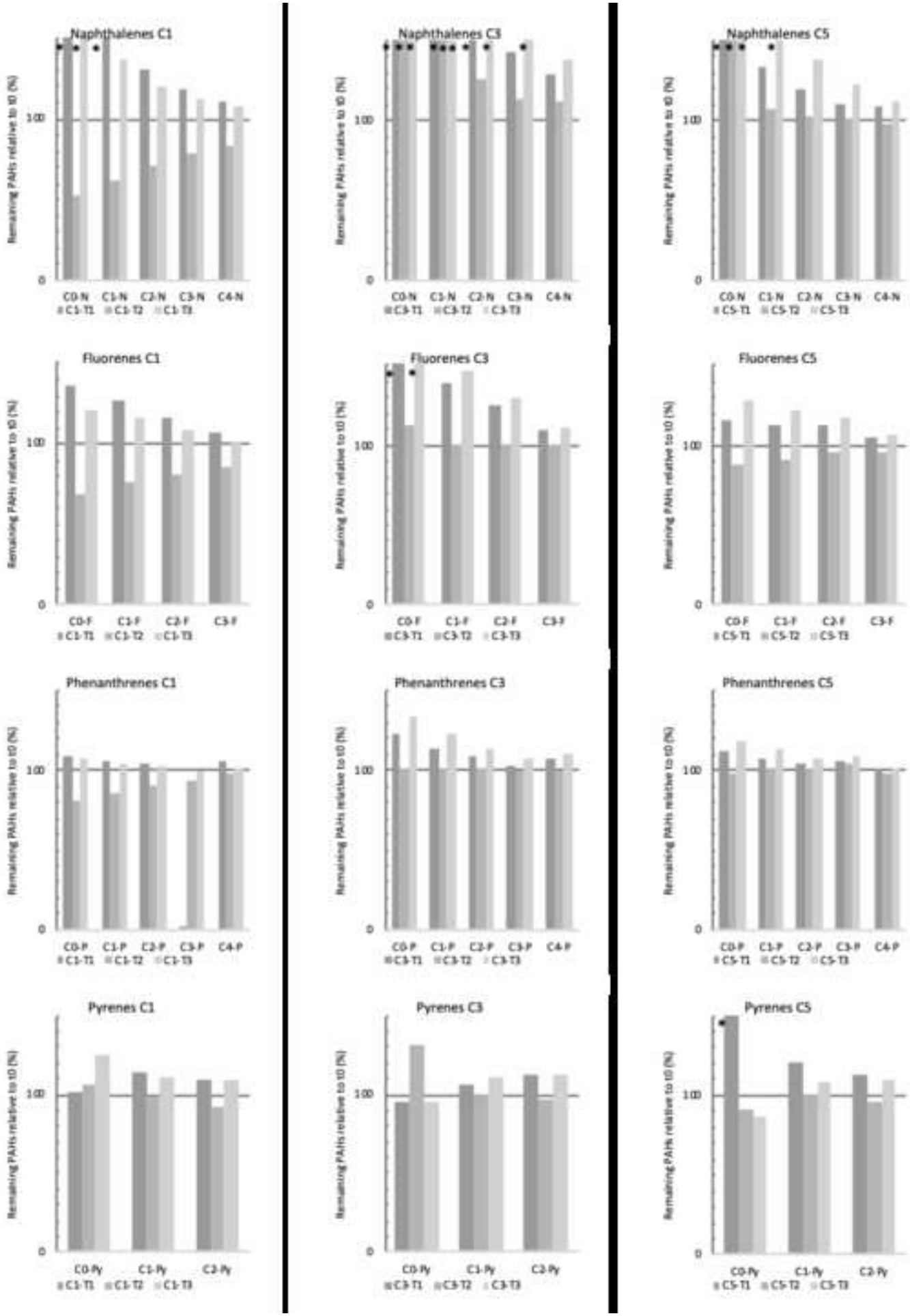

Figure 6

Click here to download high resolution image

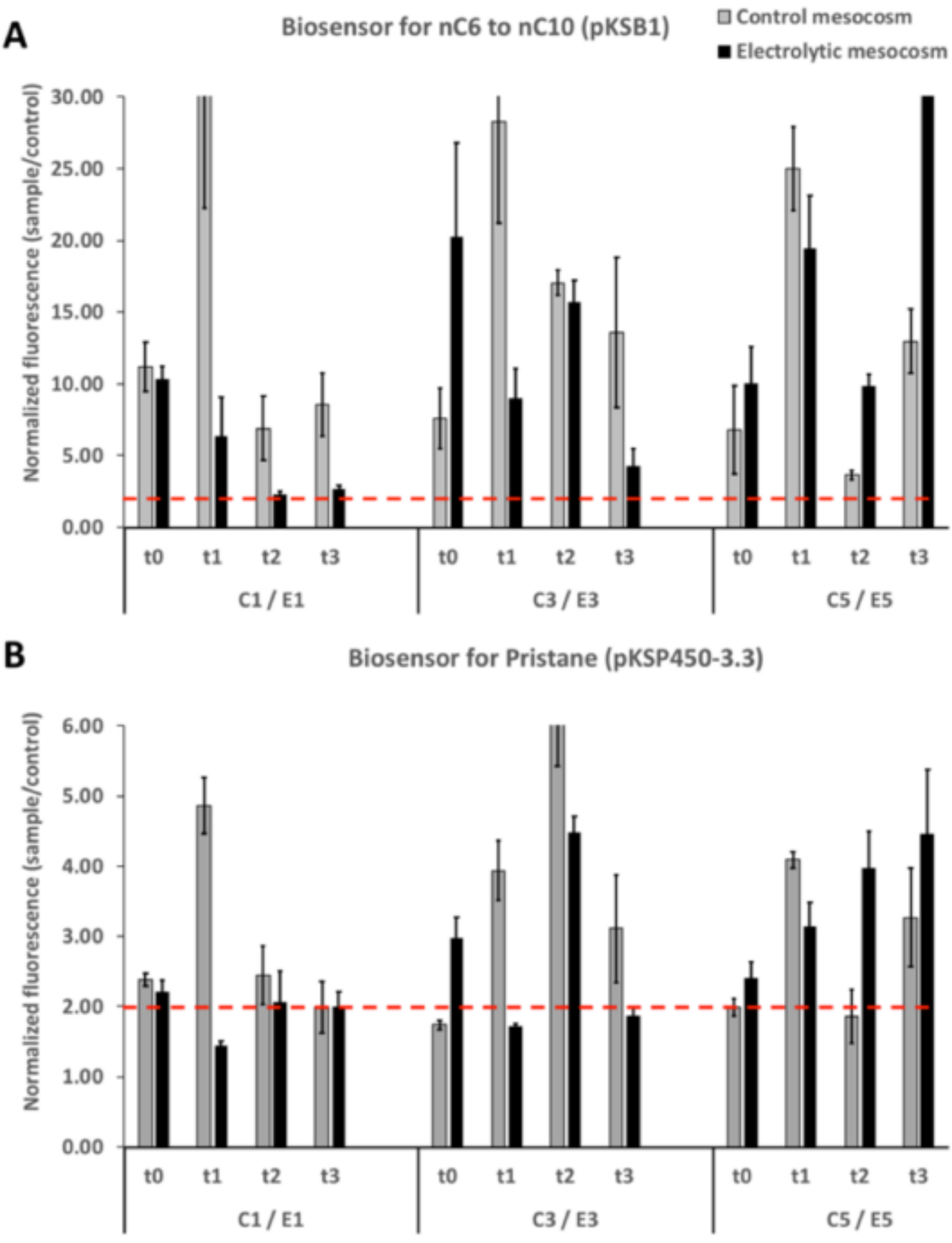

Figure 7

Click here to download high resolution image

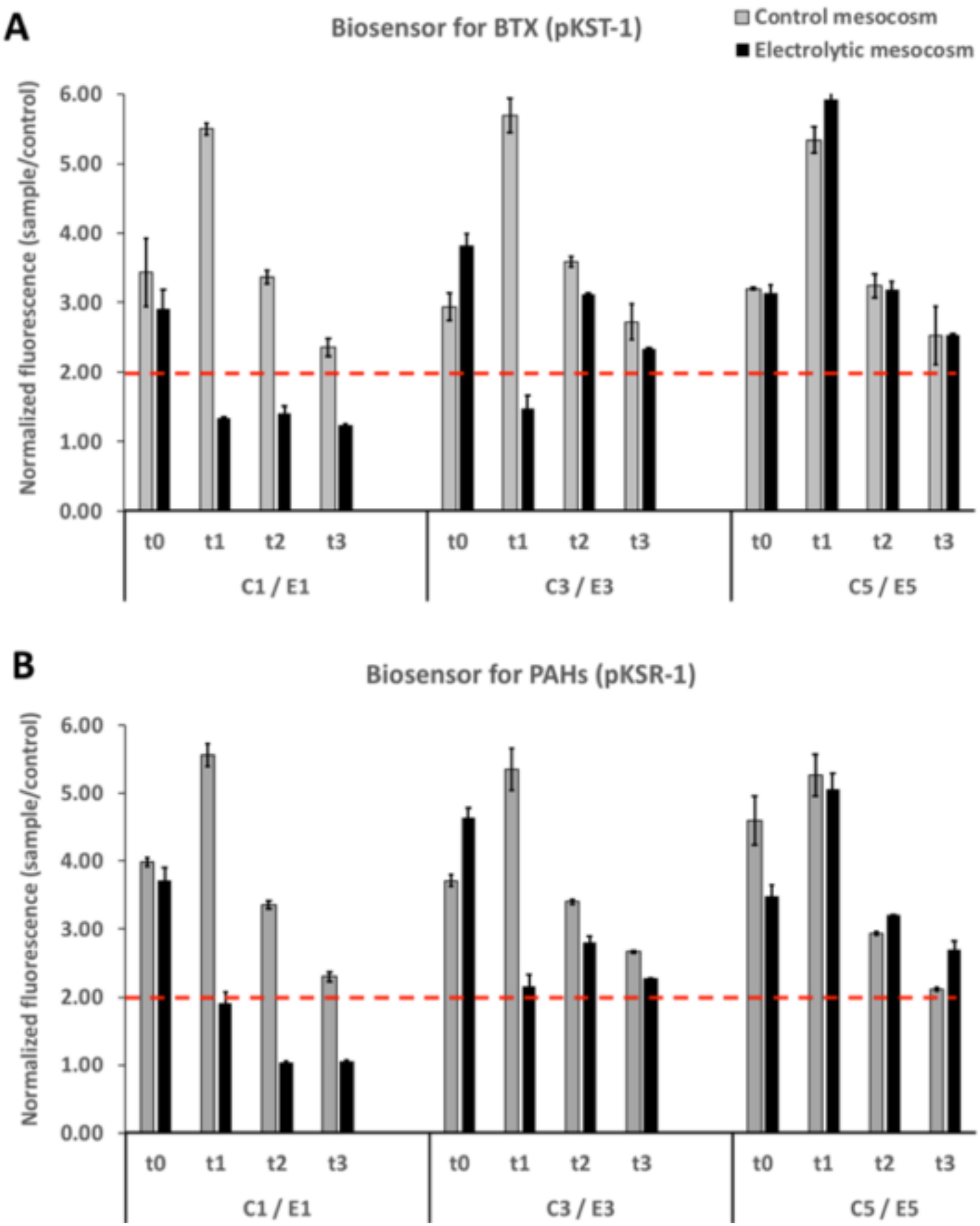

Figure 8

Click here to download high resolution image

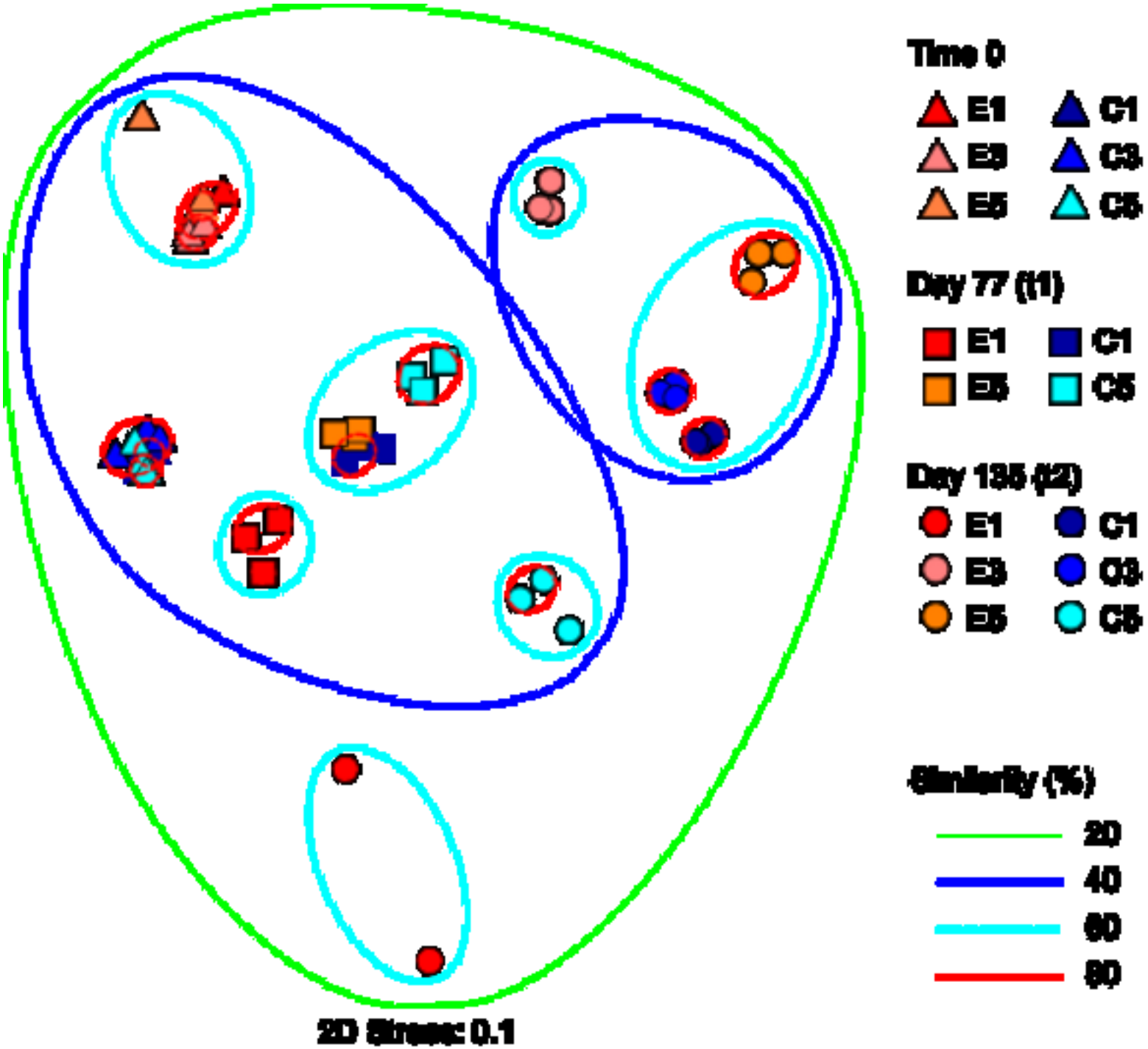

Figure 9

Click here to download high resolution image

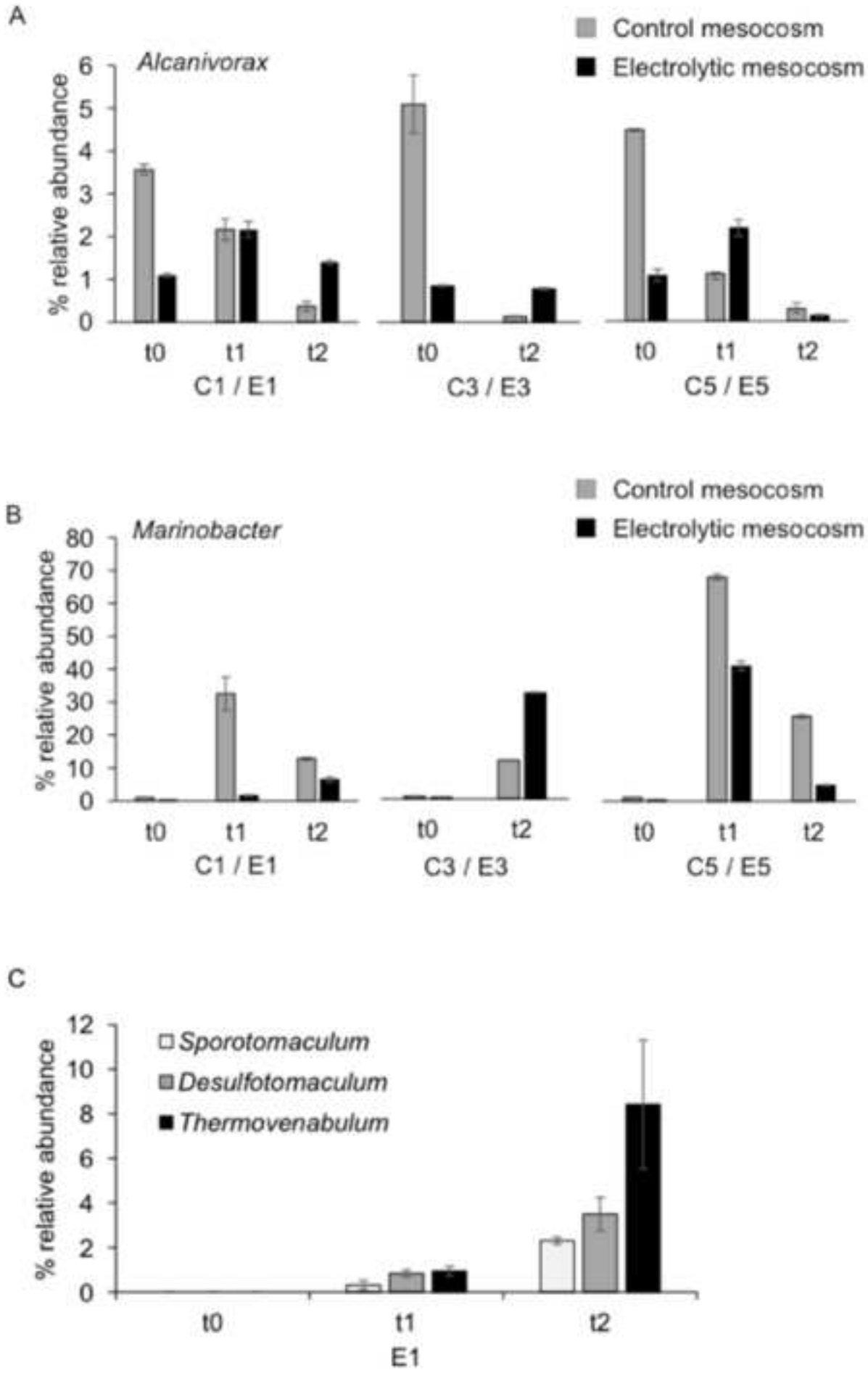

Figure 10

Click here to download high resolution image

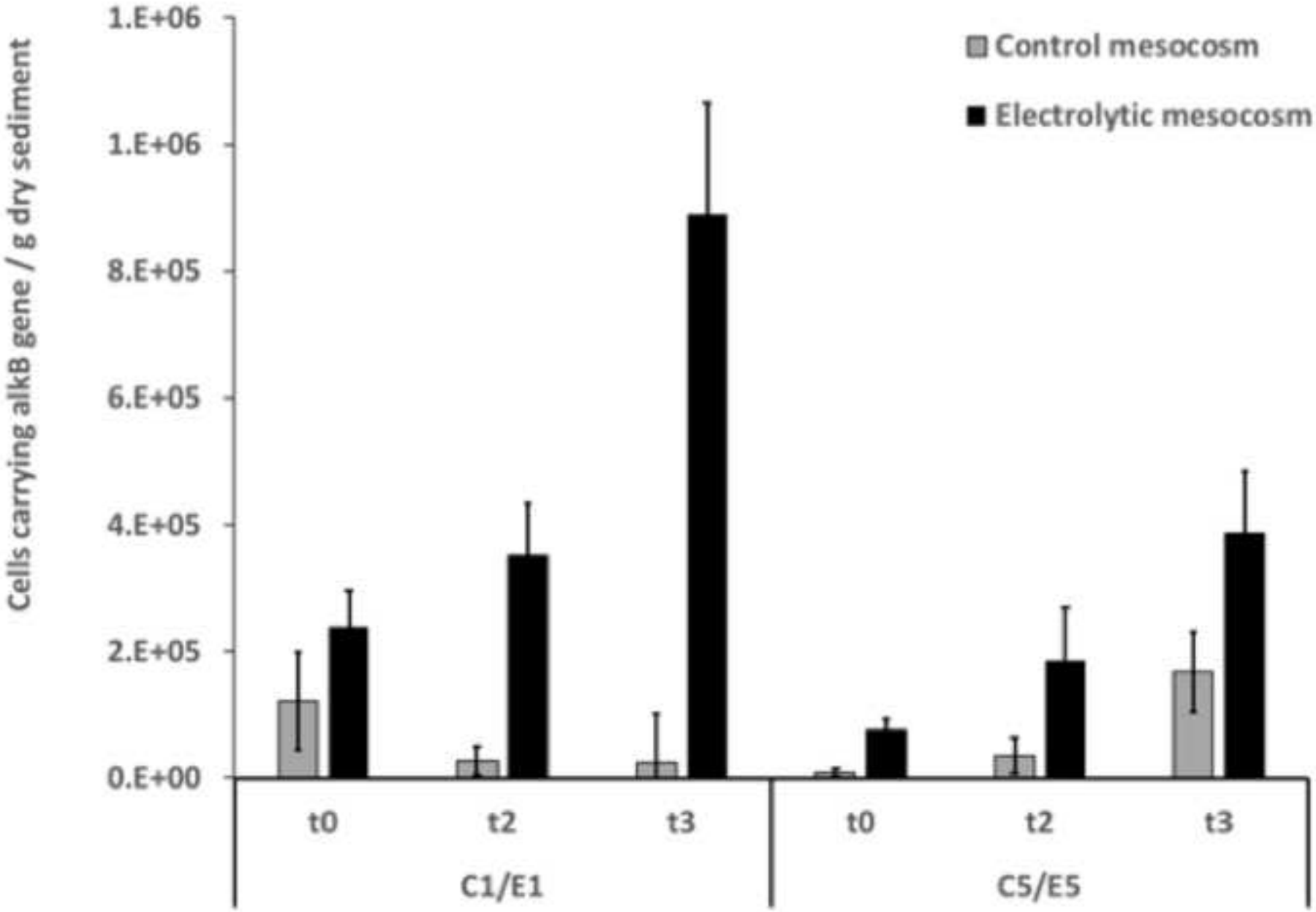

Figure 11

Click here to download high resolution image

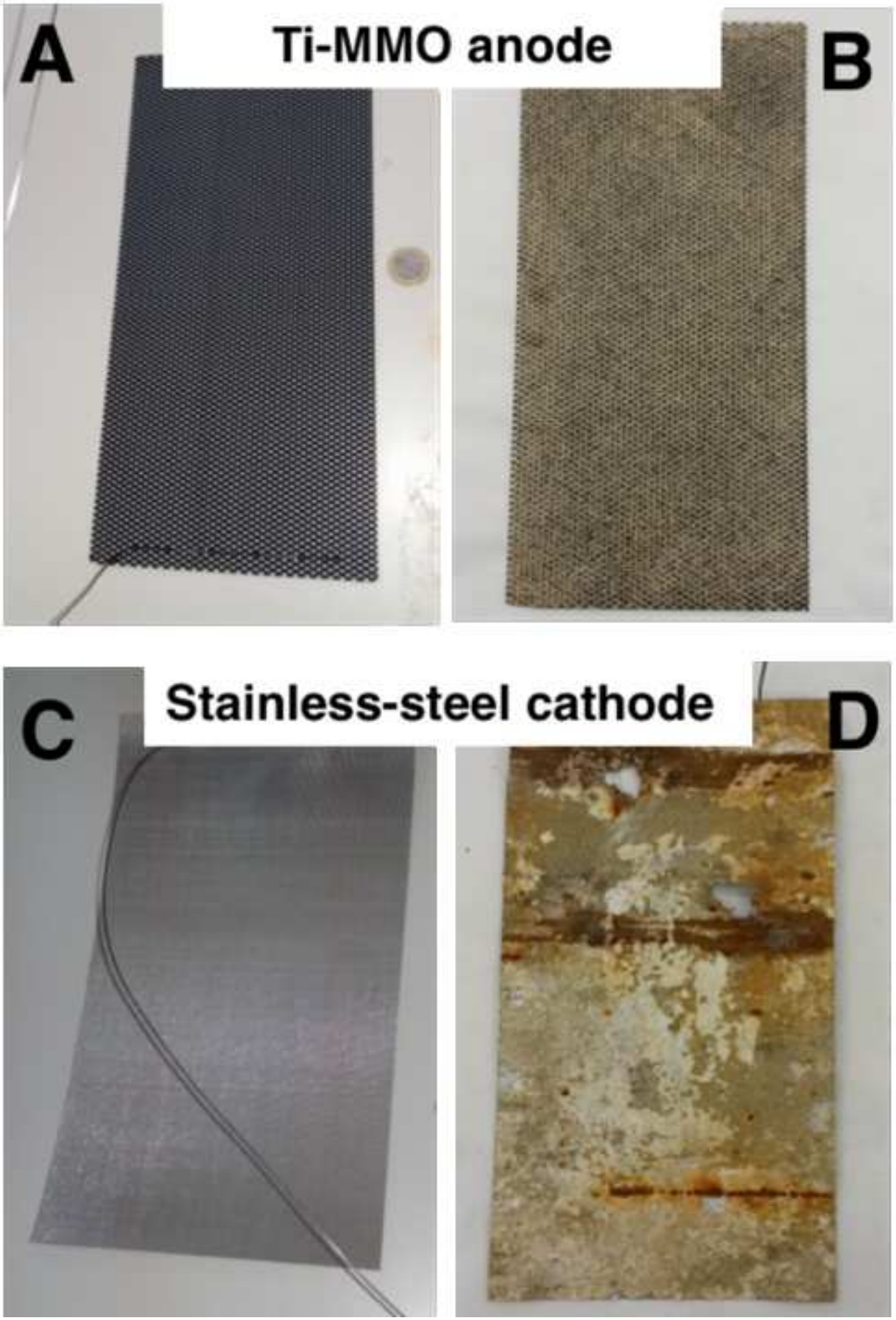

Electronic Supplementary Material (for online publication only)

Click here to download Electronic Supplementary Material (for online publication only): SUPPLEMENTARY MATERIAL.pdf

***Conflict of Interest**

Declaration of interests

☒ The authors declare that they have no known competing financial interests or personal relationships that could have appeared to influence the work reported in this paper.

☐The authors declare the following financial interests/personal relationships which may be considered as potential competing interests: